# The GPIbα intracellular tail - role in transducing VWF- and Collagen/GPVI-mediated signaling

Adela Constantinescu-Bercu[1], Yuxiao A Wang[1], Kevin J Woollard[2], Pierre Mangin[3], Karen Vanhoorelbeke[4], James TB Crawley[1] and Isabelle I Salles-Crawley[1]

[1]*Centre for Haematology, Department of Immunology and Inflammation, Imperial College London, London, UK*

[2]*Centre for Inflammatory Disease, Department of Immunology and Inflammation, Imperial College London, London, UK*

[3]*Université de Strasbourg, INSERM, EFS Grand-Est, BPPS UMR-S 1255, FMTS, Strasbourg, France*

[4] *Laboratory for Thrombosis Research, KU Leuven, Kortrijk, Belgium.*

**Correspondence:**

Isabelle I Salles-Crawley, PhD

Centre for Haematology

Department of Immunology and Inflammation

Imperial College London

5th Floor Commonwealth Building

Hammersmith Hospital Campus

Du Cane Road

London

W12 0NN

UK

Tel: +44 (0)20 8383 2298

Email: i.salles@imperial.ac.uk

**Acknowledgements**

**Authorship Contributions**

A.C-B designed and performed experiments, analyzed data and wrote the manuscript; Y.A.W performed experiments and revised the manuscript; K.J.W. designed and performed experiments and revised the manuscript; P.M and K.V. provided critical reagents and revised the manuscript; J.T.B.C designed experiments, prepared the figures and wrote the manuscript; I.I.S-C designed and performed experiments, analyzed data, prepared the figures and wrote the manuscript.


**Disclosure of Conflicts of Interest**

The authors declare no competing financial interests.

**Abstract**

The GPIb$\alpha$-VWF A1 domain interaction is essential for platelet tethering under high shear. Synergy between GPIb$\alpha$ and GPVI signaling machineries has been suggested previously, however its molecular mechanism remains unclear. We generated a novel *GPIb$\alpha$* transgenic mouse (*GpIb$\alpha^{\Delta sig/\Delta sig}$*) by CRISPR-Cas9 technology to delete the last 24 residues of the GPIb$\alpha$ intracellular tail that harbors the 14-3-3 and phosphoinositide-3 kinase binding sites. *GPIb$\alpha^{\Delta sig/\Delta sig}$* platelets bound VWF normally under flow. However, they formed fewer filopodia on VWF/botrocetin in the presence of a $\alpha_{IIb}\beta_3$ blocker, demonstrating that despite normal ligand binding, VWF-dependent signaling is diminished. Activation of *GpIb$\alpha^{\Delta sig/\Delta sig}$* platelets with ADP and thrombin was normal, but *GpIb$\alpha^{\Delta sig/\Delta sig}$* platelets stimulated with collagen-related-peptide (CRP) exhibited markedly decreased P-selectin exposure and $\alpha_{IIb}\beta_3$ activation, suggesting a role for the GpIb$\alpha$ intracellular tail in GPVI-mediated signaling. Consistent with this, while haemostasis was normal in *GPIb$\alpha^{\Delta sig/\Delta sig}$* mice, diminished tyrosine-phosphorylation, (particularly pSYK) was detected in CRP-stimulated *GpIb$\alpha^{\Delta sig/\Delta sig}$* platelets as well as reduced platelet spreading on CRP. Platelet responses to rhodocytin were also affected in *GpIb$\alpha^{\Delta sig/\Delta sig}$* platelets but to a lesser extent than those with CRP. *GpIb$\alpha^{\Delta sig/\Delta sig}$* platelets formed smaller aggregates than wild-type platelets on collagen-coated microchannels at low, medium and high shear. In response to both VWF and collagen binding, flow assays performed with plasma-free blood or in the presence of $\alpha_{IIb}\beta_3$- or GPVI-blockers suggested reduced $\alpha_{IIb}\beta_3$ activation contributes to the phenotype of the *GpIb$\alpha^{\Delta sig/\Delta sig}$* platelets. Together, these results reveal a new role for the intracellular tail of GPIb$\alpha$ in transducing both VWF-GPIb$\alpha$ and collagen-GPVI signaling events in platelets.

**Article summary**

GPIb$\alpha$ and GPVI are two key receptors on the platelet surface. Using a novel transgenic mouse (*GPIb$\alpha^{\Delta sig/\Delta sig}$*) that lacks the last 24 amino acids of the GPIb$\alpha$ intracellular tail, we demonstrate the importance of this region not only in transducing signals in response to GPIb$\alpha$ binding to VWF, but also for collagen-GPVI-mediated platelet responses revealing previously underappreciated receptor crosstalk between GPIb$\alpha$ and GPVI.

**Introduction**

To fulfil their hemostatic function, platelets are recruited to sites of vessel damage by von Willebrand factor (VWF), which interacts with exposed collagen and, thereafter, to glycoprotein (GP) Ib$\alpha$ on the platelet via its A1 domain. VWF-mediated platelet tethering facilitates platelet capture.[1] Subsequent interaction of platelets with additional ligands (e.g. $\alpha_{IIb}\beta_3$-fibrinogen, collagen-GPVI, collagen-$\alpha_2\beta_1$) and changes in platelet phenotype are required to stabilize the platelet plug. Although the VWF-GPIb$\alpha$ interaction primarily facilitates platelet recruitment, it also transduces a signal that causes intraplatelet $Ca^{2+}$ release and activation of the platelet integrin, $\alpha_{IIb}\beta_3$.[2-5] These signaling events are highly dependent upon flow as shear forces induce unfolding of the GPIb$\alpha$ mechanosensitive juxtamembrane region that translates the mechanical signal into intracellular biochemical events.[6, 7] Signaling is dependent upon the binding of adaptor and signaling molecules (e.g. Src kinases, Lyn and c-Src, 14-3-3 isoforms and phosphoinositide-3 kinase - PI3K) that can associate with the GPIb$\alpha$ intracellular tail.[8-12] Downstream activation of PLC$\gamma$2, PI3K-Akt, cGMP-PKG, mitogen activated kinase and LIM kinase 1 pathways have also been reported.[13-19] By comparison to other platelet agonists (e.g. collagen, thrombin, ADP, thromboxane A2), signaling through GPIb$\alpha$ is considered weak. VWF-GPIb$\alpha$ signaling, which we term platelet 'priming' rather than activation, does not induce appreciable degranulation.[5] Therefore, the contribution of platelet 'priming' to normal hemostasis remains unclear as the effects of the other platelet agonists have the potential to mask those of GPIb$\alpha$. However, in scenarios where other platelet agonists are either absent or in low abundance (e.g. platelet recruitment to endothelial or bacterial surfaces), the effects/importance of GPIb$\alpha$ signaling may become more prominent.[5]

GPVI is a collagen/fibrin receptor on the platelet surface that non-covalently associates with Fc receptor $\gamma$-chain (FcR$\gamma$) and signals via immunoreceptor tyrosine-based activation motifs (ITAM).[20-22] Collagen binding to platelets induces clustering of GPVI, which results in the phosphorylation of FcR$\gamma$ by Src family kinases, Lyn and Fyn, that associate with the intracellular domain of GPVI.[23, 24] This causes the recruitment and phosphorylation of Syk tyrosine kinase, and formation of a LAT-based signaling complex that can activate phospholipase C (PLC) $\gamma$2 and lead to release of intraplatelet $Ca^{2+}$ stores, activation of protein kinase (PK) C, and ultimately $\alpha_{IIb}\beta_3$ activation and both $\alpha$- and dense-granule release.[21]

Previous studies have suggested functional associations between GPIb$\alpha$ and GPVI and/or its co-receptor FcR$\gamma$.[13, 25, 26] For example, VWF-GPIb$\alpha$-mediated platelet responses are reportedly impaired in GPVI/FcR$\gamma$ deficiencies in both mice and humans.[13, 27] There is also evidence that VWF can potentiate responses after collagen mediated responses in human platelets.[28] However, the molecular basis of GPIb$\alpha$ and GPVI receptor crosstalk has not been elucidated. Using a novel GPIb$\alpha$ transgenic mouse in which the last 24 amino acids (a.a.) of the GPIb$\alpha$ intracellular tail were deleted, we demonstrate the importance of this region not only to VWF-dependent signaling in platelets, but also reveal a major contribution in augmenting GPVI-mediated platelet signaling.

**Methods**

**Mice**

All procedures were performed with the United Kingdom Home Office approval in accordance with the Animals (Scientific Procedures) Act of 1986. *Gplbα*$^{Δsig/Δsig}$ mice were generated in-house by the Medical Research Council transgenic group at Imperial College using CRISPR-Cas9 technology (Figure 1). Briefly, pronuclear injections (CBAB6F1) were performed with Cas9 mRNA (75ng/µl), guide RNAs (gRNAs; 25-50ng/µl) and single-strand oligo donor DNA (25-50ng/µl). The donor DNA (GGTAAGGCCTAATGGGCGAGTGGGGCCTCTGGTAGCAGGACGGCGACCCTGAGCTCTGAGTC AGGGTCGTGGTCAGGACCTATTGGGCACAGTGGGCATTA) had 50 bp homology arms at the 5' and 3' ends (Integrated DNA Technologies). Embryos were transferred to pseudo-pregnant CBAB6F1 female mice. Two founder mice originated from the same gRNA (CGACCCTGACTCAGAGCTGAGGG) were bred with C57BL/6 mice. F1 *Gplbα*$^{Δsig/+}$ mice were bred to obtain *Gplbα*$^{Δsig/Δsig}$ mice, and *Gplbα*$^{+/+}$ littermates were used as controls. Genotyping was performed by PCR amplification of a *Gplbα* fragment (551bp) using primers: AAGCACTCACACCACAAGCC and AGTATGAATGAGCGGGAGCC and subsequent Sanger sequencing (Genewiz).

Experimental procedures were performed as previously described. (29, 30) Additional details are included in the Online Supplementary Appendix.

**Results**

***Generation of Gplbα*$^{Δsig/Δsig}$ *mice***

Sequence identity between human and murine GPIbα intracellular region is very high, supporting the contention that their functions are well conserved (Figure 1A). To evaluate the role of the GPIbα intracellular tail upon both VWF- and collagen/GPVI-mediated signaling, we generated a novel transgenic mouse (*Gplbα*$^{Δsig/Δsig}$) using CRISPR-Cas9 technology. We introduced a point mutation (Ser695Stop) that resulted in a premature stop codon that deletes the last 24 a.a. of the GPIbα intracellular tail (a.a. 695-718) containing the entire 14-3-3 isoform and PI3K binding region, (10, 12) but maintains the upstream filamin binding site in GPIbα (residues 668-681 in murine GPIbα)(31) (Figure 1A-B). Introduction of the mutation was confirmed by sequencing and by Western blotting using an anti-GPIbα antibody that recognizes the terminal region of the intracellular tail (Figure 1C-E). *Gplbα*$^{Δsig/Δsig}$ mice were viable and born with the expected Mendelian frequencies.

***Gplbα*$^{Δsig/Δsig}$ *mice platelet count, platelet size and hemostatic function***

*Gplbα*$^{Δsig/Δsig}$ mice had mildly reduced (~20%) platelet counts and slightly larger platelet size (Figure 2A-B), but other haematological parameters were unaffected (Online Supplementary Table S1). This is in contrast to the severe thrombocytopenia and giant platelets observed in complete *Gplbα*

5

deficiency in mice or Bernard-Soulier patients.(32, 33) Expression of the major platelet receptors, GPVI, $\alpha_{IIb}\beta_3$, GPIbβ, and the extracellular region of GPIbα was unaltered on *GpIbα*$^{Δsig/Δsig}$ platelet surfaces (Figure 2C).

To assess haemostatic function in *GpIbα*$^{Δsig/Δsig}$ mice, we performed tail bleeding assays. Unlike *Vwf*$^{-/-}$ mice or mice lacking the extracellular domains of GPIbα,(32, 34, 35) *GpIbα*$^{Δsig/Δsig}$ mice displayed normal blood loss following tail transection (Figure 2D), suggesting that *GpIbα*$^{Δsig/Δsig}$ platelets can be recruited to sites of vessel damage similar to wild-type mice.

There was no difference between *GpIbα*$^{Δsig/Δsig}$ mice and wild-type littermates in a non-ablative laser-induced thrombus formation, as measured by the kinetics and extent, of both platelet accumulation and fibrin deposition (Figure 2-E-G;  Online Supplementary Figure S1 & Video 1).(29, 30, 36). These results support the contention that deletion of the GPIbα does not appreciably influence either platelet recruitment or their ability to support thrombin generation. In this model, platelet accumulation requires both VWF and thrombin but has less dependency upon collagen exposure or GPVI signaling due to the non-ablative injury. (37, 38)

### *GpIbα*$^{Δsig/Δsig}$ platelets bind VWF normally, but exhibit decreased VWF-mediated signaling

To specifically examine the effect of the GPIbα intracellular tail truncation upon VWF-dependent platelet capture, we coated microchannels with murine VWF over which we perfused plasma-free blood (to remove fibrinogen and outside-in activation $\alpha_{IIb}\beta_3$) at 1000s$^{-1}$. *GpIbα*$^{Δsig/Δsig}$ platelets were recruited normally to murine VWF-coated surfaces with rolling velocities, surface coverage and platelet accumulation unaltered compared to *GpIbα*$^{+/+}$ platelets (Figure 3A-D; Video 2).

To investigate the impact of the deletion of the last 24 a.a. of GPIbα on VWF signaling, we performed platelet spreading assays on murine VWF, which rely upon VWF-GPIbα signaling. On VWF alone, very few *GpIbα*$^{+/+}$ or *GpIbα*$^{Δsig/Δsig}$ platelets bound to VWF and only very few exhibited filopodia (Figure 3E-H). When these experiments were repeated in the presence of botrocetin (a snake venom that increases the affinity of VWF A1 domain for GPIbα)(39) a large proportion (90%±2.8) of *GpIbα*$^{+/+}$ platelets underwent shape changes and developed filopodia (Figure 3E and 3G; Online Supplementary Figure S2A-B), a well-described consequence of VWF-GPIbα signaling.(9, 19) This process was significantly diminished in *GpIbα*$^{Δsig/Δsig}$ platelets with only 46%±2.6 platelets exhibiting filopodia (Figure 3E and 3G; Online Supplementary Figure S2C-D).(9, 19) When experiments were performed in the presence of both botrocetin and GR144053, which competitively inhibits the interaction of $\alpha_{IIb}\beta_3$ with VWF and/or fibrinogen, the number of *GpIbα*$^{+/+}$ platelets forming filopodia was not appreciably influenced (Online Supplementary Figure S2B), but the proportion of that formed >3 filopodia was significantly reduced (37%±6.7 vs. 74%±6.9) (Online Supplementary Figure S2A), revealing the contribution of outside-in signaling to filopodia formation. Under these conditions, here again although *GpIbα*$^{Δsig/Δsig}$ platelets bound VWF surfaces, they had a significantly diminished ability to form filopodia (Figure 3E and H). Moreover, GR144053 had no effect upon filopodia formation in *GpIbα*$^{Δsig/Δsig}$ platelets (Online Supplementary Figure S2C), suggesting that the reduced filopodia

formation in these platelets was likely due to a defect in VWF-GPIbα signaling manifest by a lack of activation of $\alpha_{IIb}\beta_3$ in response to VWF-GPIbα binding. Taken together, these results indicate that deletion of the last 24 a.a. of the intracellular tail of GPIbα does not influence platelet binding to VWF, but significantly reduces VWF-GPIbα downstream signaling response including $\alpha_{IIb}\beta_3$ activation.

### The intracellular tail of GPIbα is important for GPVI signaling

We next evaluated agonist-induced platelet activation in *GpIbα<sup>Δsig/Δsig</sup>* mice. In response to ADP, washed *GpIbα<sup>Δsig/Δsig</sup>* platelets exhibited normal $\alpha_{IIb}\beta_3$ activation and P-selectin exposure and normal platelet aggregation (Figure 4A-D). Responses to thrombin were also normal except for a slight significant decrease in P-selectin exposure with the lowest thrombin concentration (Figure 4A-B) but this did not influence thrombin-induced platelet aggregation (Figure 4C-D). How this reduced P-selectin exposure in response to low thrombin concentration is manifest remains unclear, but may reflect the findings of a previous study that suggested the importance of 14-3-3ζ binding to GPIbα specifically for low-dose thrombin responses.(40) Despite largely unaffected responses to ADP and thrombin, in response to collagen-related peptide (CRP), *GpIbα<sup>Δsig/Δsig</sup>* platelets exhibited markedly reduced $\alpha_{IIb}\beta_3$ activation and P-selectin exposure (Figure 4A-B). Interestingly, *GpIbα<sup>Δsig/Δsig</sup>* platelet aggregation following CRP stimulation appeared normal (Figure 4C-D).

Next, we evaluated the ability of *GpIbα<sup>Δsig/Δsig</sup>* platelets to spread on fibrinogen surfaces with and without prior stimulation with thrombin. Without platelet stimulation, similar to wild-type platelets, most *GpIbα<sup>Δsig/Δsig</sup>* platelets remained round while upon stimulation with thrombin ~80% platelets spread fully with no difference observed in the spread platelet area (Online Supplementary Figure S3A-E). As full spreading is highly dependent upon outside-in signaling through $\alpha_{IIb}\beta_3$,(41) this suggests that this signaling pathway is unaffected in *GpIbα<sup>Δsig/Δsig</sup>* platelets. We then explored the ability of platelets to spread on CRP-coated surfaces. Consistent with diminished platelet activation in response to CRP, *GpIbα<sup>Δsig/Δsig</sup>* platelets remained round in contrast to wild-type platelets (59%±3.4 versus 19%±7; Figure 4E and 4G). This effect was also quantified by a 20% reduction in bound platelet area (Figure 4F) and in the reduced incidence of filopodia formation - 16%±6.3 for *GpIbα<sup>Δsig/Δsig</sup>* vs 52%±7.1 for *GpIbα<sup>+/+</sup>* (Figure 4E and 4G). Collectively, these results reveal an appreciable defect in GPVI-mediated signaling in *GpIbα<sup>Δsig/Δsig</sup>* platelets.

There was an overall reduction in tyrosine phosphorylation after CRP stimulation in *GpIbα<sup>Δsig/Δsig</sup>* platelets compared to wild-type platelets (Figure 4H). Further analysis revealed appreciably reduced Syk kinase activation in *GpIbα<sup>Δsig/Δsig</sup>* platelets, as measured by phosphorylation of Syk on Tyr525 and Tyr526 in response to CRP and lower phosphorylation levels of its downstream target pPLCγ2 (p-Tyr 1217), although this was less marked than for those observed with pSyk (Figure 4I-K). In addition, phosphorylation levels of Akt (p-Ser 473), a known substrate of PI3K were also appreciably diminished in *GpIbα<sup>Δsig/Δsig</sup>* vs *GpIbα<sup>Δsig/Δsig</sup>* (Figure 4I and 4L). To assess whether the effect of truncation of GPIbα was specific for GPVI-mediated platelet responses, or whether other tyrosine-

mediated signaling pathways might also be affected, we stimulated *GpIbα$^{Δsig/Δsig}$* and wild-type platelets with rhodocytin (C-type lectin receptor 2 (CLEC-2) agonist). Tyrosine-phosphorylation profile of *GpIbα$^{Δsig/Δsig}$* platelets in response to rhodocytin was similar to that of *GpIbα$^{+/+}$* platelets, with slightly reduced phosphorylation of Syk (~20%) (Online Supplementary Figure S4A-C). P-selectin exposure in response to rhodocytin was reduced in *GpIbα$^{Δsig/Δsig}$* platelets while $α_{IIb}β_3$ activation was only diminished for the lowest concentration of the toxin without reaching statistical significance (Online Supplementary Figure S4D-E). These results suggest that the GPIbα tail may also influence CLEC-2 ITAM-mediated signaling, but perhaps with reduced dependency.

### The role of the GPIbα intracellular tail in platelet recruitment and aggregation under flow.

To examine the consequences of the combined effects of disrupted VWF-GPIbα signaling and diminished GPVI-signaling in platelets in more physiological assays, we quantified platelet recruitment and aggregate formation on collagen-coated microchannels under flow. Experiments were performed at high (3000s$^{-1}$), medium (1000s$^{-1}$) and low (200s$^{-1}$) shear, as platelet <u>recruitment</u> is increasingly dependent on VWF-GPIbα as shear increases while subsequent platelet aggregate formation on collagen surfaces becomes more dependent upon GPVI signaling (42-44).

Perfusing whole blood at 3000s$^{-1}$ and 1000s$^{-1}$ over collagen, we observed a marked reduction in surface coverage of *GpIbα$^{Δsig/Δsig}$* platelets when compared to *GpIbα$^{+/+}$* platelets (Figures 5A-B and 6A-B; Videos 3 and 4). *GpIbα$^{Δsig/Δsig}$* platelets that bound to collagen also formed smaller aggregates than *GpIbα$^{+/+}$* platelets (Figures 5C and 6C), likely reflecting the subsequent effect of diminished collagen-GPVI signaling. Perfusing wild-type plasma-free blood (to remove soluble VWF and fibrinogen) in collagen-coated microchannels revealed a significant reduction of both platelet adhesion and thrombus growth to similar levels observed in *GpIbα$^{Δsig/Δsig}$* samples (Figure 6A-B;D-E) showing that a small amount of VWF-independent binding to collagen occurs at 1000s$^{-1}$. When whole blood experiments were performed in the presence of GR144053, to block $α_{IIb}β_3$, *GpIbα$^{+/+}$* platelets were recruited to the collagen surface as a monolayer. However, additional platelet-platelet recruitment was abolished and therefore there was limited thrombus growth in 3D. This was measured by an increase in surface coverage with a decrease in thrombus formation (i.e. total platelet fluorescence; Figure 6A-B;D).(45) Surface coverage as well as platelet accumulation of *GpIbα$^{Δsig/Δsig}$* platelets was similar in both the absence and presence of GR144053 (Figure 6A-B;E), suggesting that lack of active $α_{IIb}β_3$ is part of the platelet phenotype. To more specifically examine the role of GPVI in this system, we performed experiments in the presence of JAQ1, an anti-murine GPVI blocking antibody. Blocking GPVI significantly reduced surface coverage and platelet accumulation in *GpIbα$^{Δsig/Δsig}$* and *GpIbα$^{+/+}$* platelets, revealing the important contribution of GPVI signaling at 1000s$^{-1}$ (Figure 6F-I), in stabilizing platelet recruitment and their subsequent aggregation.

At venous shear rates (200s$^{-1}$) where the dependencies on VWF and collagen are slightly different to 1000s$^{-1}$, surface coverage of *GpIbα$^{Δsig/Δsig}$* platelets was slightly reduced compared to *GpIbα$^{+/+}$* platelets although it did not reach significance. However, thrombus growth was significantly

diminished (Figure 7A-C; Video 5). Using plasma-free blood, the surface coverage was similar for *GpIbα*$^{Δsig/Δsig}$ and *GpIbα*$^{+/+}$ platelets, mediated by direct (VWF-independent) interaction with collagen (Figure 7A-B). Similar to high-shear conditions, platelet accumulation under plasma-free conditions of *GpIbα*$^{+/+}$ platelets was significantly reduced compared to whole blood (Figure 7D) similar to those observed with *GpIbα*$^{Δsig/Δsig}$ platelets (Figure 7E). In the presence of GR144053, we saw the same increase in surface coverage of *GpIbα*$^{+/+}$ platelets with reduced localized 3D-platelet thrombi (Figure 7A-B) although the platelet accumulation was not significantly different to *GpIbα*$^{+/+}$ whole blood (Figure 7D) likely due to the increased platelet coverage. Consistent with the results obtained under high-shear conditions, the effect of increased surface coverage in the presence of GR144053 was not observed with *GpIbα*$^{Δsig/Δsig}$ platelets, nor was platelet accumulation appreciably further diminished (Figure 7A-B and 7E). Finally, similar to results obtained under arterial shear conditions, blocking GPVI significantly reduced surface coverage and platelet accumulation in both *GpIbα*$^{Δsig/Δsig}$ and *GpIbα*$^{+/+}$ platelets (Figure 7F-I). As removal of either VWF or blocking of GPVI had very similar effects, this suggests that VWF-GPIbα and GPVI-collagen binding may act synergistically to recruit platelets at low shear.

**Discussion**

The ability of platelet GPIbα binding to VWF to transduce intraplatelet signaling is well-known, but the hemostatic role of the platelet 'priming' that follows has frequently been perceived as redundant due to the comparatively mild phenotypic changes in platelets that ensue when compared to other platelet agonists (e.g. thrombin, collagen). Using a novel *GpIbα*$^{Δsig/Δsig}$ mouse, we now demonstrate that the intracellular tail of GPIbα is important not only for transduction of VWF-GPIbα signaling, but also collagen-GPVI-mediated responses in platelets (Figure 8).

The binding of GPIbα to VWF, and of GPVI to collagen, are critical events for platelet plug formation.(42, 46, 47) Previous studies reported associations between GPIbα and GPVI, or its co-receptor FcRγ suggesting potential interplay between these signaling pathways.(25, 26, 28) Functional crosstalk between these signaling pathways is supported by the diminished VWF-GPIbα-dependent responses in platelets deficient in GPVI and by the ability of VWF to further potentiate platelet secretion in response to CRP.(13, 27, 28)

To explore GPIbα signaling function and its influence upon GPVI signaling, we generated *GpIbα*$^{Δsig/Δsig}$ mice by introduction of a stop codon downstream of the main filamin binding site (a.a. 668-681), but upstream of the 14-3-3 isoforms and PI3K binding regions that are important for VWF-GPIbα signaling.(8-12, 48)(Figure 1) This resulted in uniform production of platelets that express GPIbα with truncated intracellular tail. This circumvented the limitations associated with studying/expressing platelet receptor complexes in heterologous cellular systems. Previously generated full knockout (*GpIbα*$^{-/-}$) and also *GpIbα/IL4Rα*-tg mice that lack the extracellular region of GPIbα do not enable analysis of VWF signaling per se, as they lack the ability to bind VWF, meaning

that one cannot dissociate the effects of loss of VWF binding and/or VWF signaling upon functional effects upon the platelets.(32, 35) Transgenic mice (hTg$^{Y605X}$) that express human GPIbα that lacks the terminal 6 a.a. of the intracellular tail displayed reduced megakaryocyte recovery following induced thrombocytopenia,(49) but more recent *in vitro* studies have revealed that these mice do not lack the entire 14-3-3/PI3K binding region,(9, 10, 12) suggesting that their VWF signaling function may not be fully disrupted making interpretation of the mouse phenotype difficult.

*GpIbα$^{Δsig/Δsig}$* mice had a modest reduction in platelet counts compared to *GpIbα$^{+/+}$* littermates that is likely be attributable to the small increase in platelet size (Figure 2A-B). Interestingly, platelet size is also moderately increased in the *GpIbα/IL4Rα*-tg mice,(35) but, again, this is modest compared to the size observed in *GpIbα$^{-/-}$* or in Bernard-Soulier platelets.(32, 33) Although the major filamin binding site remains intact in *GpIbα$^{Δsig/Δsig}$* mice, our findings may be consistent with CHO cell studies that suggested the presence of additional or extended filamin binding regions within intracellular tail of GPIbα.(48) By themselves, the 20% reduction in platelet count and slight increase in platelet size would not impart a hemostatic defect.(50)

*GpIbα$^{Δsig/Δsig}$* mice exhibited normal hemostatic responses to tail transection, and normal thrombus formation following mild laser-induced thrombosis (Figure 2D-G). We used a non-perforating endothelial cell injury that does not induce collagen exposure. Therefore, this non-ablasive model is independent of collagen-mediated signaling pathways. (36, 38) However, both the tail transection and laser-induced models are sensitive to VWF function.(34, 37) Our results reveal the normal VWF-binding function of *GpIbα$^{Δsig/Δsig}$* platelets. Normal bleeding times were also reported in *hTg$^{Y605X}$* transgenic mice with no overt effect on platelet or coagulation functions.(49)

Truncation of the intracellular tail of GPIbα did not alter expression of its extracellular domain (nor influence surface expression of GPIbβ, GPVI or α$_{IIb}$β$_3$) (Figure 2C). Consequently, *GpIbα$^{Δsig/Δsig}$* platelet capture to mouse VWF-coated surfaces was unaffected as well their rolling velocities (Figure 3A-D). Despite normal VWF binding, deletion of the PI3K and 14-3-3 binding region in GPIbα (9, 10, 12) significantly decreased filopodia extension upon stimulation of VWF binding with botrocetin but also in the presence of an α$_{IIb}$β$_3$ antagonist that prevent outside-in signaling induced by the VWF C4 domain binding to activated α$_{IIb}$β$_3$ (Figure 3E;G-H)). Normal VWF-platelet binding in *GpIbα$^{Δsig/Δsig}$* mice is in line with previous studies showing that deletion of the 14-3-3ζ binding site in human GPIbα in GPIb-IX CHO cells does not influence VWF binding, but does reduce their ability to spread.(9, 51) Other studies showed that a membrane-permeable inhibitor of the 14-3-3ζ-GPIbα interaction (MP-αC) inhibited GPIbα-dependent platelet agglutination and was protective in murine thrombosis models.(11, 52) However, although this peptide disrupts the interaction between 14-3-3ζ and GPIbα, it may also influence 14-3-3ζ function independent of GPIbα binding. This contention is perhaps supported by a recent study revealing that 14-3-3ζ deficient mice are protected against arterial thrombosis with normal VWF-GPIbα-mediated platelet function.(53)

In addition to defective VWF-mediated signaling, *GpIbα^{Δsig/Δsig}* platelets exhibited markedly diminished collagen-mediated signaling through GPVI evidenced by reduced surface expression of P-selectin and activation of $\alpha_{IIb}\beta_3$, fewer filopodia upon CRP stimulation (Figure 4A-B;E-G), and severely diminished platelet aggregate formation on collagen under venous and arterial shears (Figures 5-7). Bernard-Soulier patient platelets have historically been reported to respond normally to collagen in aggregation assays (54). However, the thrombocytopenia and giant platelets associated with full GPIbα deficiency combined with the loss of VWF-dependent platelet recruitment on collagen impair full analysis of other platelet signaling pathways under physiological flow conditions. Interestingly, although early studies on Bernard-Soulier patients reported that platelet aggregation in response to collagen was normal, their transformation into procoagulant platelets was specifically impaired in response to collagen (but not other agonists).(55) More recently, a Bernard-Soulier patient with mutations in both GPIbα and filamin A was also reported to exhibit defects in GPVI-mediated signaling responses.(56) Although the authors contended that this defect might be due to the filamin A mutation, this may warrant some reappraisal in light of the data presented herein. Like Bernard-Soulier platelets, we found that *GpIbα^{Δsig/Δsig}* platelets aggregated normally in response to CRP (Figure 4C-D). The signaling deficit presumably allows sufficient activation of $\alpha_{IIb}\beta_3$ for the platelets to aggregate. This is perhaps unsurprising given that *Gp6^{+/-}* platelet aggregation is only affected at low collagen concentrations.(57, 58) Taken together, previous studies support the contention that Bernard-Soulier patient platelets exhibit a partial deficit in GPVI signaling that resembles the deficit in *GpIbα^{Δsig/Δsig}* mouse platelets.

Platelets can interact with collagen directly through GPVI and $\alpha_2\beta_1$, and indirectly via GPIbα binding to VWF, the latter being increasingly important as shear rates rise to first capture the platelets and enable the aforementioned direct interactions to take place.(42, 59) This is demonstrated in wild-type mice, similar to previous reports,(43, 60) by the markedly reduced binding of platelets to collagen in the absence of plasma (and therefore VWF) at medium shear rates (Figure 6A-B,D). Although we demonstrated that *GpIbα^{Δsig/Δsig}* platelets bind VWF normally, we saw the largest defect in platelet coverage/accumulation when compared to wild-type mice at 3000s^{-1} (Figure 5). Based on these results, it seems likely that VWF-GPIbα signaling is also important at these high shear rates, similar to the importance of GPIbα binding to VWF for platelet tethering. We therefore contend that under medium/high shear conditions, VWF-GPIbα platelet priming induces some rapid activation of $\alpha_{IIb}\beta_3$, which enable the platelets to better withstand the higher shear rates, prior to their interaction/activation by collagen (Figure 8). Although most evident at the highest shear rates, *GpIbα^{Δsig/Δsig}* platelets exhibited reduced accumulation at venous shear rates (Figures 7C). Given that the surface coverage on collagen was not significantly altered at 200s^{-1} in *GpIbα^{Δsig/Δsig}* platelets compared to wild-type platelets (Figure 7A-B), the deficit in subsequent platelet accumulation must be due to reduced reactivity of *GpIbα^{Δsig/Δsig}* platelets. This is supported by the clear importance of $\alpha_{IIb}\beta_3$ activation to this assay, demonstrated by the effects of GR144053 in preventing 3D accumulation of platelets at both 200 s^{-1} and 1000s^{-1} in wild-type platelets (Figures 6 and 7 panels A-

D). We also observed an increase in the platelet coverage in wild-type platelets in the presence of the $\alpha_{IIb}\beta_3$ blocker. This is in line with our previous study and others showing that $\alpha_{IIb}\beta_3$ blockade allows the formation of a platelet monolayer, but prevents thrombus growth in 3D and also lateral platelet-platelet aggregation (Figures 6B and 7B).(5, 45, 61, 62) This underscores the importance in quantifying both platelet coverage and accumulation in flow assays when studying platelet signaling defects.(45, 61)   Importantly, GR144053 did not alter these parameters when added to *GpIbα^{Δsig/Δsig}* platelets (Figures 6 and 7, panels A-B, D-E), demonstrating a lack of $\alpha_{IIb}\beta_3$ activation that would be consistent with a diminished GPVI-mediated signaling response. It is important to note that this response is diminished, rather than ablated as the addition of JAQ1 led to a marked decrease in both platelet tethering and accumulation at both 1000s$^{-1}$ and 200s$^{-1}$ shear rates (Figure 6F-I and Figure 7F-I).  The question remains open as to the precise contribution of VWF-GPIbα versus collagen-GPVI signaling deficits to the phenotype of *GpIbα^{Δsig/Δsig}* platelets. Our data suggest that both signaling pathways likely contribute to this, as disruption of either interaction causes a major reduction in platelet accumulation in wild-type platelets under both venous and arterial shear rates.

GPVI belongs to the immunoglobulin superfamily and signals via tyrosine kinase phosphorylation pathways. To further investigate the defect in GPVI signaling in *GpIbα^{Δsig/Δsig}* platelets, analysis of tyrosine phosphorylation downstream of GPVI revealed that SYK and PLCγ2 phosphorylation was reduced in *GpIbα^{Δsig/Δsig}* platelets (Figure 4H-K). Interestingly, the diminished phosphorylation was more pronounced for SYK than for PLCγ2 perhaps highlighting the existence of LAT-independent mechanisms of PLCγ2 phosphorylation.(63) Interestingly, activation of *GpIbα^{Δsig/Δsig}* platelets via CLEC-2, another receptor that signals via an ITAM motif,(64) was also affected, but perhaps to a lesser extent than those mediated by GPVI (Online Supplementary Figure S4) suggesting that the function of the GPIbα intracellular tail is more important for GPVI mediated responses. Based on these findings, we hypothesize that the tail of GPIbα may be important for the docking of signaling molecules such as SYK, LAT and PLCγ2 that are downstream of GPVI and CLEC-2 on ITAM phosphorylated motif of the FcRγ and CLEC-2 receptors and warrant further investigation. It would also be of interest to determine if the reduction in PI3K signaling in response to CRP stimulation (Figure 4I-L) is due to the lack of binding of PI3K to the intracellular tail of GPIbα or it is a consequence of diminished SYK phosphorylation (65)

In summary, we generated a novel GPIbα transgenic mouse in which their platelets bind VWF normally, but the subsequent VWF-GPIbα signaling is disrupted. Intriguingly, these mice clearly reveal the molecular link between GPIbα- and GPVI-mediated signaling in platelets and underscore the cooperative functions of these two major platelet receptors.(45) Platelets in addition to their important role in thrombosis and haemostasis contribute to the host response to infection and inflammation.(66-69) Our recent work suggests that VWF-GPIbα-dependent platelet priming potentiates the recruitment of neutrophils, which may represent a key early event in the targeting of pathogens, but also in the development of deep vein thrombosis.(5) The *GpIbα^{Δsig/Δsig}* mice now

provide an invaluable tool to probe the importance of the GPIbα-mediated signaling in inflammatory diseases such as atherosclerosis and deep vein thrombosis, as well as in the host response to infection but also to fully decipher the molecular dependency of GPVI signaling upon GPIbα.

**References**

1. Li R. The Glycoprotein Ib-IX-V Complex
 Vol. 4th. Michelson AD, Cattaneo M, Frelinger L, Newman PJ. Elsevier/Academic Press; 2018. (Platelets).

2. Mazzucato M, Pradella P, Cozzi MR, De Marco L, Ruggeri ZM. Sequential cytoplasmic calcium signals in a 2-stage platelet activation process induced by the glycoprotein Ibalpha mechanoreceptor. Blood. 2002;100(8):2793-2800.

3. Nesbitt WS, Kulkarni S, Giuliano S, et al. Distinct glycoprotein Ib/V/IX and integrin alpha IIbbeta 3-dependent calcium signals cooperatively regulate platelet adhesion under flow. J Biol Chem. 2002;277(4):2965-2972.

4. Kasirer-Friede A, Cozzi MR, Mazzucato M, et al. Signaling through GP Ib-IX-V activates alpha IIb beta 3 independently of other receptors. Blood. 2004;103(9):3403-3411.

5. Constantinescu-Bercu A, Grassi L, Frontini M, et al. Activated alphaIIbbeta3 on platelets mediates flow-dependent NETosis via SLC44A2. Elife. 2020;9:53353.

6. Zhang W, Deng W, Zhou L, et al. Identification of a juxtamembrane mechanosensitive domain in the platelet mechanosensor glycoprotein Ib-IX complex. Blood. 2015;125(3):562-569.

7. Ju L, Chen Y, Xue L, Du X, Zhu C. Cooperative unfolding of distinctive mechanoreceptor domains transduces force into signals. Elife. 2016;5:e15447.

8. Gu M, Xi X, Englund GD, Berndt MC, Du X. Analysis of the roles of 14-3-3 in the platelet glycoprotein Ib-IX-mediated activation of integrin alpha(IIb)beta(3) using a reconstituted mammalian cell expression model. J Cell Biol. 1999;147(5):1085-1096.

9. Mangin P, David T, Lavaud V, et al. Identification of a novel 14-3-3zeta binding site within the cytoplasmic tail of platelet glycoprotein Ibalpha. Blood. 2004;104(2):420-427.

10. Mangin PH, Receveur N, Wurtz V, et al. Identification of five novel 14-3-3 isoforms interacting with the GPIb-IX complex in platelets. J Thromb Haemost. 2009;7(9):1550-1555.

11. Dai K, Bodnar R, Berndt MC, Du X. A critical role for 14-3-3zeta protein in regulating the VWF binding function of platelet glycoprotein Ib-IX and its therapeutic implications. Blood. 2005;106(6):1975-1981.

12. Mu FT, Andrews RK, Arthur JF, et al. A functional 14-3-3zeta-independent association of PI3-kinase with glycoprotein Ib alpha, the major ligand-binding subunit of the platelet glycoprotein Ib-IX-V complex. Blood. 2008;111(9):4580-4587.

13. Wu Y, Suzuki-Inoue K, Satoh K, et al. Role of Fc receptor gamma-chain in platelet glycoprotein Ib-mediated signaling. Blood. 2001;97(12):3836-3845.

14. Li Z, Zhang G, Feil R, Han J, Du X. Sequential activation of p38 and ERK pathways by cGMP-dependent protein kinase leading to activation of the platelet integrin alphaIIb beta3. Blood. 2006;107(3):965-972.

15. Li Z, Xi X, Gu M, et al. A stimulatory role for cGMP-dependent protein kinase in platelet activation. Cell. 2003;112(1):77-86.

16. Yin H, Liu J, Li Z, et al. Src family tyrosine kinase Lyn mediates VWF/GPIb-IX-induced platelet activation via the cGMP signaling pathway. Blood. 2008;112(4):1139-1146.

17. Garcia A, Quinton TM, Dorsam RT, Kunapuli SP. Src family kinase-mediated and Erk-mediated thromboxane A2 generation are essential for VWF/GPIb-induced fibrinogen receptor activation in human platelets. Blood. 2005;106(10):3410-3414.

18. Estevez B, Stojanovic-Terpo A, Delaney MK, et al. LIM kinase-1 selectively promotes glycoprotein Ib-IX-mediated TXA2 synthesis, platelet activation, and thrombosis. Blood. 2013;121(22):4586-4594.

19. Mangin P, Yuan Y, Goncalves I, et al. Signaling role for phospholipase C gamma 2 in platelet glycoprotein Ib alpha calcium flux and cytoskeletal reorganization. Involvement of a pathway distinct from FcR gamma chain and Fc gamma RIIA. J Biol Chem. 2003;278(35):32880-32891.

20. Tsuji M, Ezumi Y, Arai M, Takayama H. A novel association of Fc receptor gamma-chain with glycoprotein VI and their co-expression as a collagen receptor in human platelets. J Biol Chem. 1997;272(38):23528-23531.

21. Rayes J, Watson SP, Nieswandt B. Functional significance of the platelet immune receptors GPVI and CLEC-2. J Clin Invest. 2019;129(1):12-23.

22. Alshehri OM, Hughes CE, Montague S, et al. Fibrin activates GPVI in human and mouse platelets. Blood. 2015;126(13):1601-1608.

23. Schmaier AA, Zou Z, Kazlauskas A, et al. Molecular priming of Lyn by GPVI enables an immune receptor to adopt a hemostatic role. Proc Natl Acad Sci U S A. 2009;106(50):21167-21172.

24. Ezumi Y, Shindoh K, Tsuji M, Takayama H. Physical and functional association of the Src family kinases Fyn and Lyn with the collagen receptor glycoprotein VI-Fc receptor gamma chain complex on human platelets. J Exp Med. 1998;188(2):267-276.

25. Falati S, Edmead CE, Poole AW. Glycoprotein Ib-V-IX, a receptor for von Willebrand factor, couples physically and functionally to the Fc receptor gamma-chain, Fyn, and Lyn to activate human platelets. Blood. 1999;94(5):1648-1656.

26. Arthur JF, Gardiner EE, Matzaris M, et al. Glycoprotein VI is associated with GPIb-IX-V on the membrane of resting and activated platelets. Thromb Haemost. 2005;93(4):716-723.

27. Goto S, Tamura N, Handa S, et al. Involvement of glycoprotein VI in platelet thrombus formation on both collagen and von Willebrand factor surfaces under flow conditions. Circulation. 2002;106(2):266-272.

28. Baker J, Griggs RK, Falati S, Poole AW. GPIb potentiates GPVI-induced responses in human platelets. Platelets. 2004;15(4):207-214.

29. Salles-Crawley I, Monkman JH, Ahnstrom J, Lane DA, Crawley JT. Vessel wall BAMBI contributes to hemostasis and thrombus stability [Research Support, N.I.H., Extramural
Research Support, Non-U.S. Gov't]. Blood. 2014;123(18):2873-2881.

30. Crawley JTB, Zalli A, Monkman JH, et al. Defective fibrin deposition and thrombus stability in Bambi(-/-) mice are mediated by elevated anticoagulant function. J Thromb Haemost. 2019;17(11):1935-1949.

31. Nakamura F, Pudas R, Heikkinen O, et al. The structure of the GPIb-filamin A complex. Blood. 2006;107(5):1925-1932.

32. Ware J, Russell S, Ruggeri ZM. Generation and rescue of a murine model of platelet dysfunction: the Bernard-Soulier syndrome. Proc Natl Acad Sci U S A. 2000;97(6):2803-2808.

33. Lanza F. Bernard-Soulier syndrome (hemorrhagiparous thrombocytic dystrophy). Orphanet J Rare Dis. 2006;1:46.

34. Denis C, Methia N, Frenette PS, et al. A mouse model of severe von Willebrand disease: defects in hemostasis and thrombosis [Research Support, Non-U.S. Gov't
Research Support, U.S. Gov't, P.H.S.]. Proc Natl Acad Sci U S A. 1998;95(16):9524-9529.

35. Kanaji T, Russell S, Ware J. Amelioration of the macrothrombocytopenia associated with the murine Bernard-Soulier syndrome. Blood. 2002;100(6):2102-2107.

36. Stalker TJ. Mouse laser injury models: variations on a theme. Platelets. 2020;31(4):423-431.

37. Dubois C, Panicot-Dubois L, Gainor JF, Furie BC, Furie B. Thrombin-initiated platelet activation in vivo is vWF independent during thrombus formation in a laser injury model. J Clin Invest. 2007;117(4):953-960.

38. Dubois C, Panicot-Dubois L, Merrill-Skoloff G, Furie B, Furie BC. Glycoprotein VI-dependent and -independent pathways of thrombus formation in vivo. Blood. 2006;107(10):3902-3906.

39. Fukuda K, Doggett T, Laurenzi IJ, Liddington RC, Diacovo TG. The snake venom protein botrocetin acts as a biological brace to promote dysfunctional platelet aggregation. Nat Struct Mol Biol. 2005;12(2):152-159.

40. Estevez B, Kim K, Delaney MK, et al. Signaling-mediated cooperativity between glycoprotein Ib-IX and protease-activated receptors in thrombin-induced platelet activation. Blood. 2016;127(5):626-636.

41. Durrant TN, van den Bosch MT, Hers I. Integrin alphaIIbbeta3 outside-in signaling. Blood. 2017;130(14):1607-1619.

42. Ruggeri ZM. The role of von Willebrand factor in thrombus formation. Thromb Res. 2007;120 Suppl 1:S5-9.

43. Kuijpers MJ, Schulte V, Oury C, et al. Facilitating roles of murine platelet glycoprotein Ib and alphaIIbbeta3 in phosphatidylserine exposure during vWF-collagen-induced thrombus formation. J Physiol. 2004;558(Pt 2):403-415.

44. Nieswandt B, Brakebusch C, Bergmeier W, et al. Glycoprotein VI but not alpha2beta1 integrin is essential for platelet interaction with collagen. EMBO J. 2001;20(9):2120-2130.

45. Pugh N, Simpson AM, Smethurst PA, et al. Synergism between platelet collagen receptors defined using receptor-specific collagen-mimetic peptide substrata in flowing blood. Blood. 2010;115(24):5069-5079.

46. Bergmeier W, Piffath CL, Goerge T, et al. The role of platelet adhesion receptor GPIbalpha far exceeds that of its main ligand, von Willebrand factor, in arterial thrombosis. Proc Natl Acad Sci U S A. 2006;103(45):16900-16905.

47. Nieswandt B, Pleines I, Bender M. Platelet adhesion and activation mechanisms in arterial thrombosis and ischaemic stroke. J Thromb Haemost. 2011;9 Suppl 1:92-104.

48. Feng S, Resendiz JC, Lu X, Kroll MH. Filamin A binding to the cytoplasmic tail of glycoprotein Ibalpha regulates von Willebrand factor-induced platelet activation. Blood. 2003;102(6):2122-2129.

49. Kanaji T, Russell S, Cunningham J, et al. Megakaryocyte proliferation and ploidy regulated by the cytoplasmic tail of glycoprotein Ibalpha. Blood. 2004;104(10):3161-3168.

50. Morowski M, Vogtle T, Kraft P, et al. Only severe thrombocytopenia results in bleeding and defective thrombus formation in mice. Blood. 2013;121(24):4938-4947.

51. David T, Strassel C, Eckly A, et al. The platelet glycoprotein GPIbbeta intracellular domain participates in von Willebrand factor induced-filopodia formation independently of the Ser 166 phosphorylation site. J Thromb Haemost. 2010;8(5):1077-1087.

52. Yin H, Stojanovic-Terpo A, Xu W, et al. Role for platelet glycoprotein Ib-IX and effects of its inhibition in endotoxemia-induced thrombosis, thrombocytopenia, and mortality. Arterioscler Thromb Vasc Biol. 2013;33(11):2529-2537.

53. Schoenwaelder SM, Darbousset R, Cranmer SL, et al. 14-3-3zeta regulates the mitochondrial respiratory reserve linked to platelet phosphatidylserine exposure and procoagulant function. Nat Commun. 2016;7:12862.

54. Andrews RK, Berndt MC. Bernard-Soulier syndrome: an update. Semin Thromb Hemost. 2013;39(6):656-662.

55. Walsh PN, Mills DC, Pareti FI, et al. Hereditary giant platelet syndrome. Absence of collagen-induced coagulant activity and deficiency of factor-XI binding to platelets. Br J Haematol. 1975;29(4):639-655.

56. Li J, Dai K, Wang Z, et al. Platelet functional alterations in a Bernard-Soulier syndrome patient with filamin A mutation. J Hematol Oncol. 2015;8:79.

57. Kato K, Kanaji T, Russell S, et al. The contribution of glycoprotein VI to stable platelet adhesion and thrombus formation illustrated by targeted gene deletion [Research Support, U.S. Gov't, P.H.S.]. Blood. 2003;102(5):1701-1707.

58. Mazharian A, Wang YJ, Mori J, et al. Mice lacking the ITIM-containing receptor G6b-B exhibit macrothrombocytopenia and aberrant platelet function. Sci Signal. 2012;5(248):ra78.

59. Nieswandt B, Watson SP. Platelet-collagen interaction: is GPVI the central receptor? Blood. 2003;102(2):449-461.

60. Kuijpers MJ, Schulte V, Bergmeier W, et al. Complementary roles of glycoprotein VI and alpha2beta1 integrin in collagen-induced thrombus formation in flowing whole blood ex vivo. FASEB J. 2003;17(6):685-687.

61. Pugh N, Maddox BD, Bihan D, et al. Differential integrin activity mediated by platelet collagen receptor engagement under flow conditions. Thromb Haemost. 2017;117(8):1588-1600.

62. Verkleij MW, Morton LF, Knight CG, et al. Simple collagen-like peptides support platelet adhesion under static but not under flow conditions: interaction via alpha2 beta1 and von Willebrand factor with specific sequences in native collagen is a requirement to resist shear forces. Blood. 1998;91(10):3808-3816.

63. Pasquet JM, Gross B, Quek L, et al. LAT is required for tyrosine phosphorylation of phospholipase cgamma2 and platelet activation by the collagen receptor GPVI. Mol Cell Biol. 1999;19(12):8326-8334.

64. Suzuki-Inoue K, Inoue O, Ozaki Y. Novel platelet activation receptor CLEC-2: from discovery to prospects. J Thromb Haemost. 2011;9 Suppl 1:44-55.

65. Manne BK, Badolia R, Dangelmaier C, et al. Distinct pathways regulate Syk protein activation downstream of immune tyrosine activation motif (ITAM) and hemITAM receptors in platelets. J Biol Chem. 2015;290(18):11557-11568.

66. Clark SR, Ma AC, Tavener SA, et al. Platelet TLR4 activates neutrophil extracellular traps to ensnare bacteria in septic blood. Nat Med. 2007;13(4):463-469.

67. Deppermann C, Kubes P. Platelets and infection. Semin Immunol. 2016;28(6):536-545.

68. Jenne CN, Kubes P. Platelets in inflammation and infection. Platelets. 2015;26(4):286-292.

69. Kapur R, Semple JW. Platelets as immune-sensing cells. Blood Adv. 2016;1(1):10-14.

**FIGURE LEGENDS:**

**Figure 1. Generation and characterization of *Gplbα*$^{\Delta sig/\Delta sig}$ mice.** (A) Sequence alignment of the last 100 amino acids (a.a.) of human and mouse GPIbα. Sequence identities are highlighted in red. Filamin binding region: (a.a. 560-573) and (a.a. 668-681) for human and mouse GPIbα; PI3K/14-3-3 binding region: (a.a. 580-610) and (a.a. 688-718) for human and mouse GPIbα. (B) Schematic representation of the *Gplbα* gene with CRISPR guide target site, gRNA sequence, BbvCI restriction enzyme site and Cas9 predicted cut site. Primers used to amplify the *Gplbα* allele from genomic DNA are indicated in purple. Design of the 101□bp ssDNA repair template with the point mutation to introduce a codon stop eliminating the BbvCI restriction enzyme site and removing the last 24 a.a. of GPIbα is also shown. The resulting truncated a.a. sequence from *Gplbα*$^{\Delta sig/\Delta sig}$ mice is indicated in green. (C) Genomic DNA sequences from *Gplbα*$^{+/+}$ and *Gplbα*$^{\Delta sig/\Delta sig}$ mice. Successful substitution is indicated with an arrow. (D) Diagram showing the binding of the anti-GPIbα tail Ab (Biorbyt; orb 215471). (E) Platelet lysates from *Gplbα*$^{+/+}$ and *Gplbα*$^{\Delta sig/\Delta sig}$ mice were probed with the anti-GPIbα tail and β-actin antibodies. Absence of band in the GPIbα western-blot confirms the successful truncation of the GPIbα intracellular tail in *Gplbα*$^{\Delta sig/\Delta sig}$ mice.

**Figure 2. *Gplbα*$^{\Delta sig/\Delta sig}$ mice display normal bleeding loss and platelet and fibrin accumulation in the laser-induced thrombosis model.** A) Platelet counts and (B) platelet size in *Gplbα*$^{+/+}$ (n=25) and *Gplbα*$^{\Delta sig/\Delta sig}$ mice (n=30) as determined by flow cytometry. (C) Surface expression of platelet receptors GPIbα, GPIbβ, $\alpha_{IIb}\beta_3$ and GPVI in *Gplbα*$^{+/+}$ and *Gplbα*$^{\Delta sig/\Delta sig}$ mice (n=4 for each genotype) determined by flow cytometry and expressed as % of control. **(**D) Bar graph analyzing blood loss after 10 min following tail transection in *Gplbα*$^{+/+}$ and *Gplbα*$^{\Delta sig/\Delta sig}$ mice (n=9 for each genotype). (E-G) Mice cremaster muscle arterioles were subjected to the laser-induced thrombosis model as described in Supplementary Methods. Curves represent median integrated fluorescence intensity (IFI) from platelets (arbitrary units: AU) (E) or fibrin(ogen) (F) as a function of time after the injury (20 thrombi in 3 *Gplbα*$^{+/+}$ and 34 thrombi in 4 *Gplbα*$^{\Delta sig/\Delta sig}$ mice). (G) Representative composite fluorescence images of platelets (green) and fibrin (red) with bright field images after laser-induced injury of the endothelium of *Gplbα*$^{+/+}$ (top panels) versus *Gplbα*$^{\Delta sig/\Delta sig}$ mice (bottom panels). Scale bar represents 10 μm. Each symbol represents one thrombus. Horizontal lines intersecting the data set represent the median. Data was analyzed using Mann Whitney test; ns: $p>0.05$. Also see Video 1 and Figure S1.

**Figure 3. *Gplbα*$^{\Delta sig/\Delta sig}$ platelets exhibit normal binding to VWF but disrupted GPIbα-mediated signaling.** (A-D) Plasma-free blood from *Gplbα*$^{+/+}$ and *Gplbα*$^{\Delta sig/\Delta sig}$ mice supplemented with anti-GPIbb-DyLight488 Ab was perfused over murine VWF at a shear rate of 1000s$^{-1}$. (A) Representative fluorescence images (n≥3; scale bar 10 μm) and bar graphs analyzing the integrated fluorescence intensity (IFI) (B) and the surface coverage (C) of *Gplbα*$^{+/+}$ and *Gplbα*$^{\Delta sig/\Delta sig}$ platelets captured by murine VWF after 3.5 mins of flow. (D) Rolling velocities (median ± CI) were calculated from (~10,000) platelets rolling/adhering to murine VWF within the first 30 seconds (n≥3) (E) Representative confocal images of *Gplbα*$^{+/+}$ and *Gplbα*$^{\Delta sig/\Delta sig}$ platelets (n=3 for each genotype) spread on mVWF and stained with Phalloidin-Alexa 488, in the absence or presence of Botrocetin or Botrocetin and GR144053 (scale bar 10 μm). (F-H) Percentage of platelets from *Gplbα*$^{+/+}$ and *Gplbα*$^{\Delta sig/\Delta sig}$ mice (individual data points representing the average of 3-6 fields of view) with no filopodia, 1-3 filopodia or >3 filopodia formed on murine VWF in the absence (F; 129 *Gplbα*$^{+/+}$ platelets and 115 *Gplbα*$^{\Delta sig/\Delta sig}$ platelets analysed) or presence of Botrocetin (G; 511 *Gplbα*$^{+/+}$ platelets and 547 *Gplbα*$^{\Delta sig/\Delta sig}$ platelets analysed), or Botrocetin and GR144053 (H; 359 *Gplbα*$^{+/+}$ platelets and 480 *Gplbα*$^{\Delta sig/\Delta sig}$ platelets analysed). Data represents mean ± SEM (B,C, F-H) or median ± CI (D) and was analyzed using unpaired two-tailed Student's t-test (B,C), unpaired Mann Whitney test (D) or using two-way ANOVA followed by Sidak's multiple comparison test (F-H); *$p<0.05$, ***$p<0.001$, ****$p<0.0001$. Also see Online Supplementary Figure S2 and Video 2.

**Figure 4: *Gplbα*$^{\Delta sig/\Delta sig}$ platelets exhibit altered GPVI-mediated signaling. (A-B)** Flow cytometric analysis of surface expression of activated $\alpha_{IIb}\beta_3$ (**A**) and P-selectin (**B**) in *Gplbα*$^{+/+}$ and *Gplbα*$^{\Delta sig/\Delta sig}$ platelets (n=8) in response to ADP (1-20μM), α-thrombin (20-200mU/ml), or CRP (1-10μg/ml). MFI: geometric mean fluorescence intensity **(C)** Representative aggregation traces (n=3-6) of washed

platelets isolated from *GpIbα*^{+/+} (blue) or *GpIbα*[Δsig/Δsig] (red) mice and stimulated with ADP (1-10µM), α-thrombin (20-50mU/ml) or CRP (0.5-3µg/ml). Aggregation was monitored using a Chronolog aggregometer over 6 mins. **(D)** Bar graph analysing the maximum aggregation (%) obtained in the conditions presented in (**C**). **(E)** Representative micrographs (n=3 for each genotype; 3 fields of view analyzed per condition; scale bar 10 µm) of 454 *GpIbα*^{+/+} and 420 *GpIbα*[Δsig/Δsig] platelets (>400) spread on CRP and stained with Phalloidin-Alexa 488. Bar graphs quantifying the surface area (**F**) and percentages (**G**) of platelets that remained round, formed filopodia or spread on CRP. **(H)** Western blot analyzing tyrosine kinase phosphorylation in platelets from *GpIbα*^{+/+} and *GpIbα*[Δsig/Δsig] mice, following stimulation with 3 µg/ml CRP for 0-180s, using β-actin as a loading control (representative of n=3). **(I)** Western blots analyzing the levels of phosphorylated and non-phosphorylated SYK, PLCγ2 and Akt in platelets from GpIbα^{+/+} and GpIbα[Δsig/Δsig] mice, after 0-180s stimulation with CRP (representative of n=3). **(J-L)** Bar graphs displaying the levels of phosphorylated SYK, PLCγ2 and Akt in platelets from GpIbα^{+/+} and GpIbα[Δsig/Δsig] mice, after 0-180s stimulation with CRP and normalizing the intensity according to the non-phosphorylated levels of SYK, PLCγ2 and Akt. For the surface area (F), the data represent the median±CI and was analyzed using the unpaired Mann Whitney test. All other data is displayed as mean±SEM and was analyzed using two-way ANOVA followed by Sidak's multiple comparison test. *$p<0.05$, **$p<0.01$, ***$p<0.001$, ****$p<0.0001$. Also see Online Supplementary Figure S2 and S3.

**Figure 5. *GpIbα*[Δsig/Δsig] platelets have a reduced ability to bind to collagen and form microthrombi at 3000s[-1].** Hirudin anticoagulated whole blood from *GpIbα*^{+/+} and *GpIbα*[Δsig/Δsig] mice was labelled with anti-GPIbβ-DyLight488 Ab and perfused over fibrillar collagen type I (0.2 mg/ml) at a shear rate of 3000s[-1] for 3 mins. **(A)** Representative fluorescence images (n=6) after 3 minutes of perfusion in whole blood (WB) from *GpIbα*^{+/+} and *GpIbα*[Δsig/Δsig] mice at 3000s[-1]. Platelet deposition **(B)** and thrombus build-up measured as integrated fluorescence intensity (IFI) (**C**). All data is shown as mean ± SEM and analyzed using unpaired two-tailed student's t-test The maximal platelet IFI was used to compare the thrombus build up data. *$p<0.05$, ***$p<0.001$. Scale bar 100 µm. Also see Video 3.
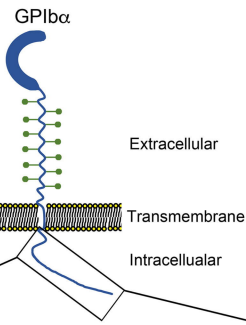
**Figure 6: *GpIbα*[Δsig/Δsig] platelets have a reduced ability to bind to collagen and form microthrombi at 1000s[-1].** **(A-E)** Hirudin anticoagulated whole blood supplemented or not with GR144053 or plasma-free blood from *GpIbα*^{+/+} and *GpIbα*[Δsig/Δsig] mice was labelled with anti-GPIbβ-DyLight488 Ab and perfused over fibrillar collagen type I (0.2 mg/ml) at a shear rate of 1000s[-1] for 3 mins. (**A**) Representative fluorescence images (n≥3) after 3 minutes of perfusion in whole blood (WB), plasma-free blood (PFB) or WB + GR144053 from *GpIbα*^{+/+} and *GpIbα*[Δsig/Δsig] mice. Platelet deposition **(B)** and thrombus build-up measured as IFI (**C-E**). All data is shown as mean ± SEM and analyzed using unpaired two-tailed student's t-test (**C**) or one-way ANOVA followed by Dunnett's multiple comparison test (**B, D-E**). Data is compared to means from *GpIbα*^{+/+} WB (**B,D**) or *GpIbα*[Δsig/Δsig] WB (**E**). The maximal platelet IFI was used to compare the thrombus build up data. *$p<0.05$. Scale bar 100 µm. Also see Video 4. **(F-I)** Hirudin anticoagulated whole blood from *GpIbα*^{+/+} and *GpIbα*[Δsig/Δsig] mice supplemented with JAQ1 or Rat-IgG control Abs (20µg/ml) was labelled with anti-GPIbβ-DyLight488 Ab and perfused over fibrillar collagen type I (0.2 mg/ml) at a shear rate of 1000s[-1] for 3 mins. **(F)** Representative fluorescence images (n=3) after 3 minutes of perfusion. Platelet deposition **(G)** and thrombus build-up measured as IFI (**H,I**). All data is shown as mean ± SEM and analyzed using unpaired two-tailed student's t-test. The maximal platelet IFI was used to compare the thrombus build up data. *$p<0.05$, **$p<0.01$. Scale bar 100 µm.

**Figure 7: *GpIbα*[Δsig/Δsig] platelets have a reduced ability to bind to collagen and form microthrombi at 200s[-1].** **(A-E)** Hirudin anticoagulated whole blood supplemented or not with GR144053 or plasma-free blood from *GpIbα*^{+/+} and *GpIbα*[Δsig/Δsig] mice was labelled with anti-GPIbβ-DyLight488 Ab and perfused over fibrillar collagen type I (0.2 mg/ml) at a shear rate of 200s[-1] for 3 mins. (**A**) Representative fluorescence images (n≥3) after 3 minutes of perfusion in whole blood (WB), plasma-free blood (PFB) or WB + GR144053 from *GpIbα*^{+/+} and *GpIbα*[Δsig/Δsig] mice. Platelet deposition **(B)** and thrombus build-up measured as IFI (**C-E**). All data is shown as mean ± SEM and analyzed using unpaired two-tailed student's t-test (**C**) or one-way ANOVA followed by Dunnett's multiple comparison test (**B,D-E**). Data is compared to means from *GpIbα*^{+/+} WB (**B,D**) or

*GpIbα*<sup>Δsig/Δsig</sup> WB (**E**). The maximal platelet IFI was used to compare the thrombus build up data. *p<0.05, **p<0.01. Scale bar 100 µm. Also see Video 5. **(F-I)** Hirudin anticoagulated whole blood from *GpIbα*<sup>+/+</sup> and *GpIbα*<sup>Δsig/Δsig</sup> mice supplemented with JAQ1 or Rat-IgG control Abs (20µg/ml) was labelled with anti- GPIbβ-DyLight488 Ab and perfused over fibrillar collagen type I (0.2 mg/ml) at a shear rate of 1000s<sup>-1</sup> for 3 mins. **(F)** Representative fluorescence images (n=3) after 3 minutes of perfusion. Platelet deposition **(G)** and thrombus build-up measured as IFI (**H,I**). All data is shown as mean ± SEM and analyzed using unpaired two-tailed student's t-test. The maximal platelet IFI was used to compare the thrombus build up data. *p<0.05. Scale bar 100 µm.

**Figure 8: Proposed model for GPIbα-GPVI cross talk.** Under normal conditions, resting/circulating platelets (1) present $\alpha_{IIb}\beta_3$ on their surface in its closed conformation. Plasma VWF (2) circulates in its globular conformation with its A1 domain hidden, preventing interaction with platelet GPIbα. Upon vascular injury, the subendothelial extracellular matrix containing collagen becomes exposed to the blood. VWF, via its A3 domain, binds to collagen and, due to shear forces, unravels to expose its A1 domain to which platelet GPIbα binds (3). Next, mechanosensitive signaling events downstream of VWF A1-GPIbα that require the intracellular tail of GPIbα take place leading to some activation of surface $\alpha_{IIb}\beta_3$ (4) while the deceleration of platelets allows for the subsequent binding of platelets to collagen via several collagen receptors including GPVI (6). The intracellular tail of GPIbα is also crucial for optimal collagen/GPVI signaling that lead to platelet activation, shape change and granule release (7). Ultimately, additional circulating platelets will be recruited at the site of injury to form the hemostatic plug (8).
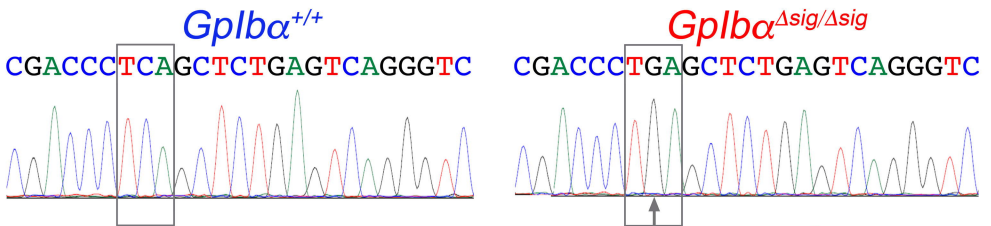
GPIbα

A

Extracellular

Transmembrane

Intracellualar

B

Filamin-binding region    14-3-3/PI3K-binding region

512                                                                                              610
Human  WVGHVKFQALDSGQGAALTTATQTTHLELQRCRQVTVPRAWLLFLRGSLPTFRSSLFLWVRPNGRVGPLVAGRRPSALSQGRGQDLLSTVSIRYSGHSL
Mouse  WTWHVTFHSLDMEQSAALALTSTHTTSLEVQRARQVTVPRAWLLFLQGSLPTFRSSLFLWVRPNGRVGPLVAGRRPSALSQGRGQDLLCTVCIRYSGHSL
620                                                                                              718

Exon 1        GpIbα        Exon 2                FW              R        primers

ORF

Cas9
BbvCI

G GTA AGG CCT AAT GGG CGA GTG GGG CCT CTG GTA GCA GGA CGG CGA CCC TCA GCT CTG AGT CAG GGT CGT GGT CAG GAC CTA TTG GGC ACA GTG GGC ATT AGG TAC TCA GGC CAT CTG TGA
C CAT TCC GGA TTA CCC GCT CAC CCC GGA CAT CGT CCT GCC GCT GGG AGT CGA GAC TCA GTC CCA GCA CCA GTC GTC CTG GAT AAC CCG TGT CAC CCG TAA TCC ATG AGT CCG GTA TCA GAC ACT

mGPIbα (679-718)   V R P N G R V G P L V A G R R P S A L S Q G R G Q D L L G T V G I R Y S G H S L stop

GGG AGU CGA GAC UCA GUC CCA GC
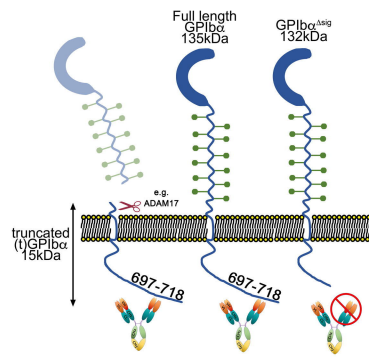gRNA

Repair DNA seq   G GTA AGG CCT AAT GGG CGA GTG GGG CCT CTG GTA GCA GGA CGG CGA CCC T G GCT CTG AGT CAG GGT CGT GGT CAG GAC CTA TTG GGC ACA GTG GGC ATT AGG TAC TCA GGC CAT CTG TGA

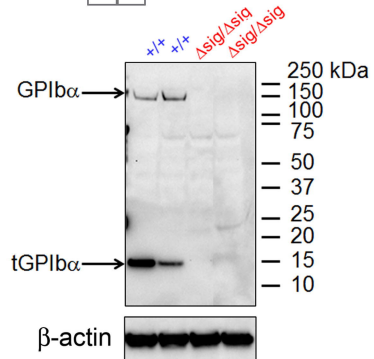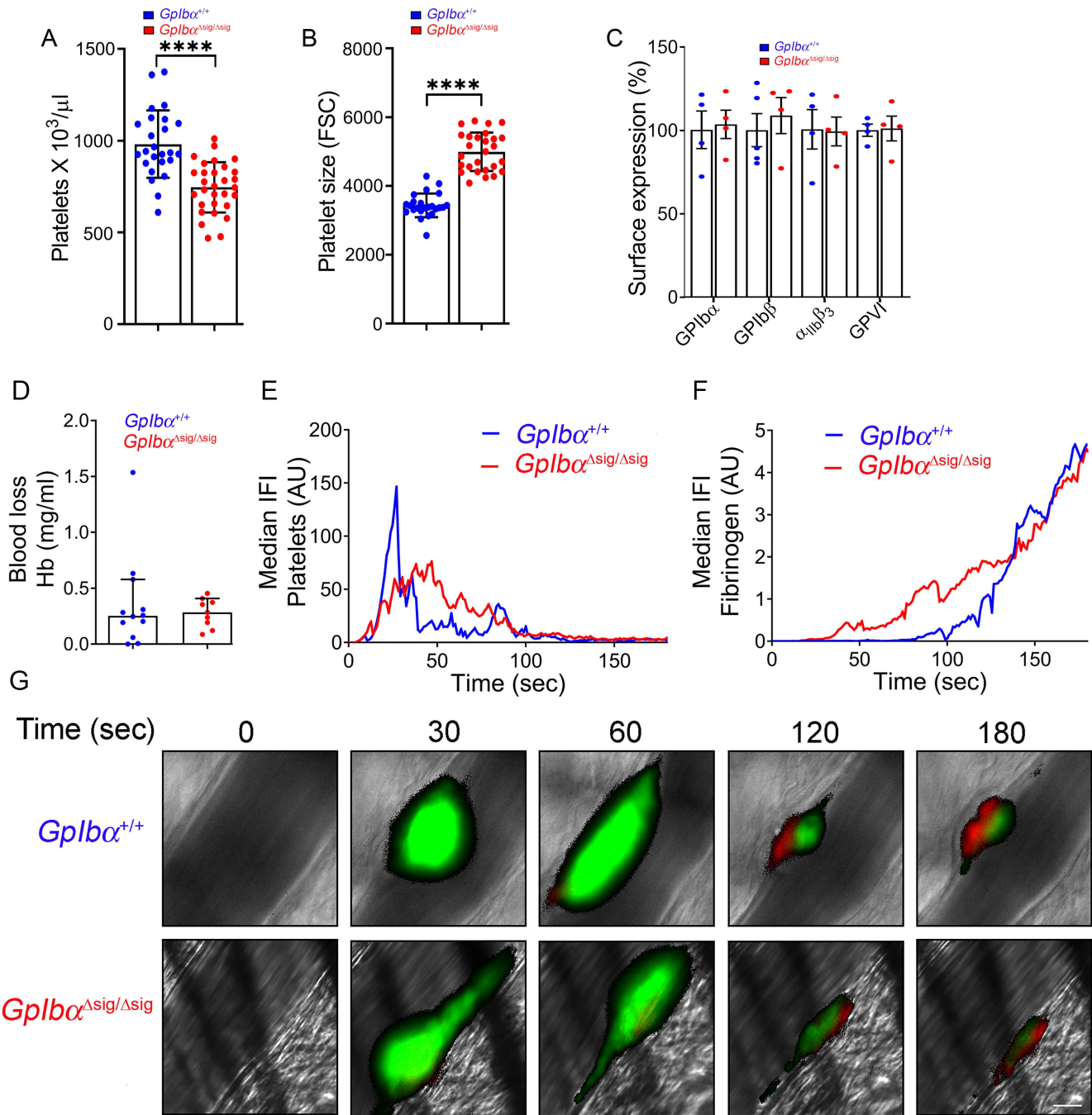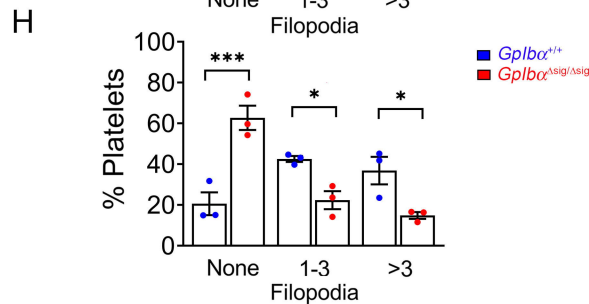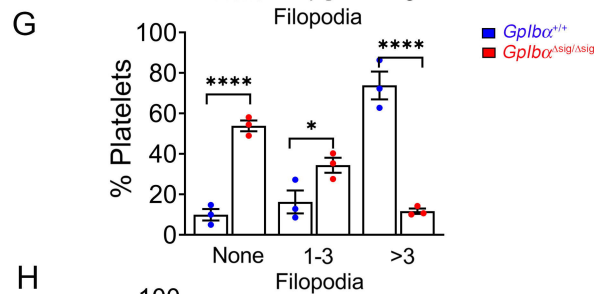mGPIbα^Δsig (679-694)   V R P N G R V G P L V A G R R P stop

C

GpIbα^+/+                                        GpIbα^Δsig/Δsig
CGACCCTCAGCTCTGAGTCAGGGTC            CGACCCTGAGCTCTGAGTCAGGGTC

D

Full length        GPIbα^Δsig
GPIbα              132kDa
135kDa

truncated
(t)GPIbα
15kDa

e.g.
ADAM17

697-718        697-718

E

+/+  +/+  Δsig/Δsig  Δsig/Δsig

GPIbα →                                    250 kDa
                                           150
                                           100
                                           75

                                           50
                                           37

                                           25
tGPIbα →                                    20
                                           15
                                           10

β-actin

**A**

$3000s^{-1}$

$GPIb\alpha^{+/+}$    $GPIb\alpha^{\Delta sig/\Delta sig}$

WB

**B**  $3000s^{-1}$

Platelet surface coverage (%)

$GPIb\alpha^{+/+}$    $GPIb\alpha^{\Delta sig/\Delta sig}$

***

**C**

IFI (platelets)

$GPIb\alpha^{+/+}$
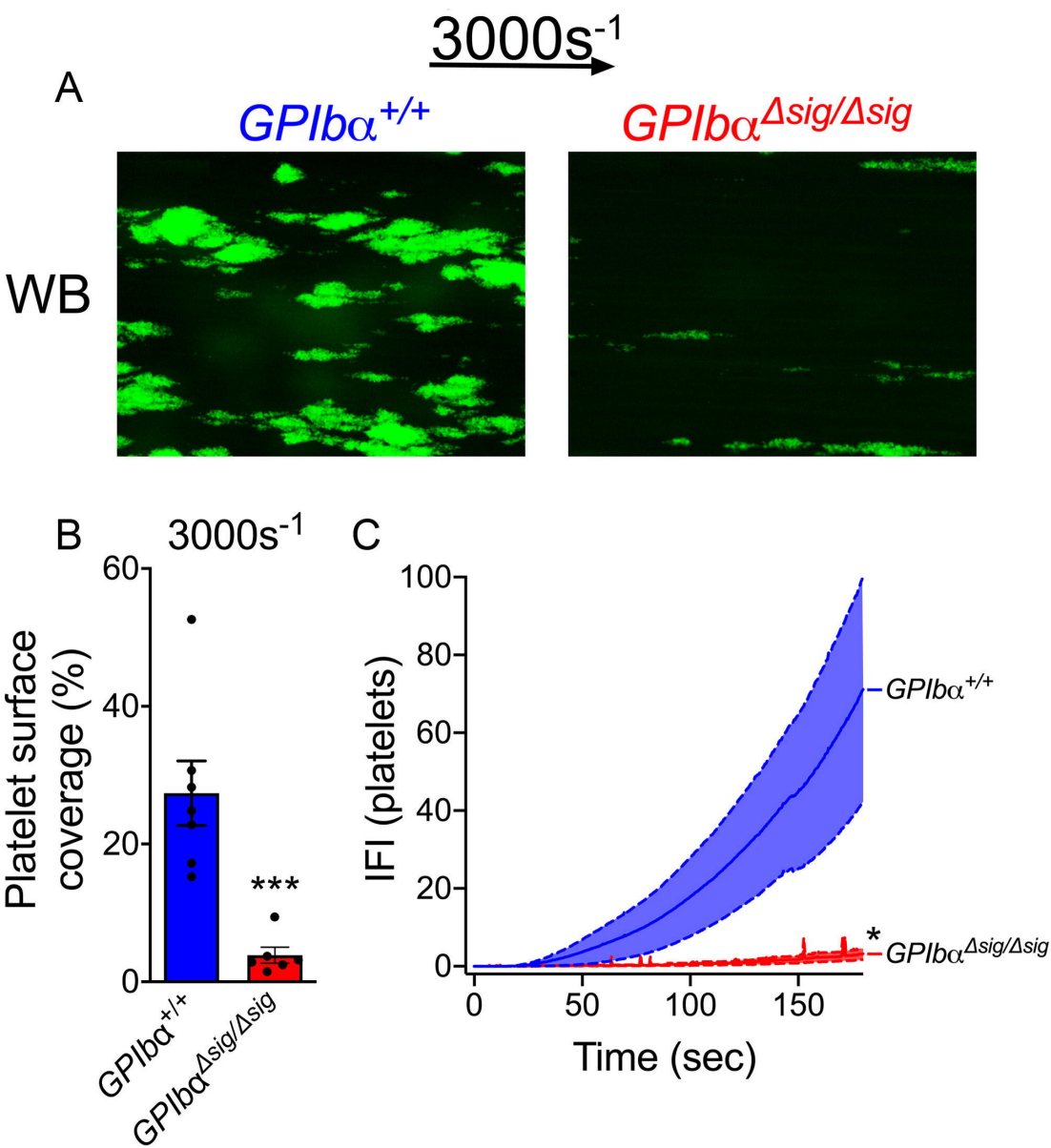
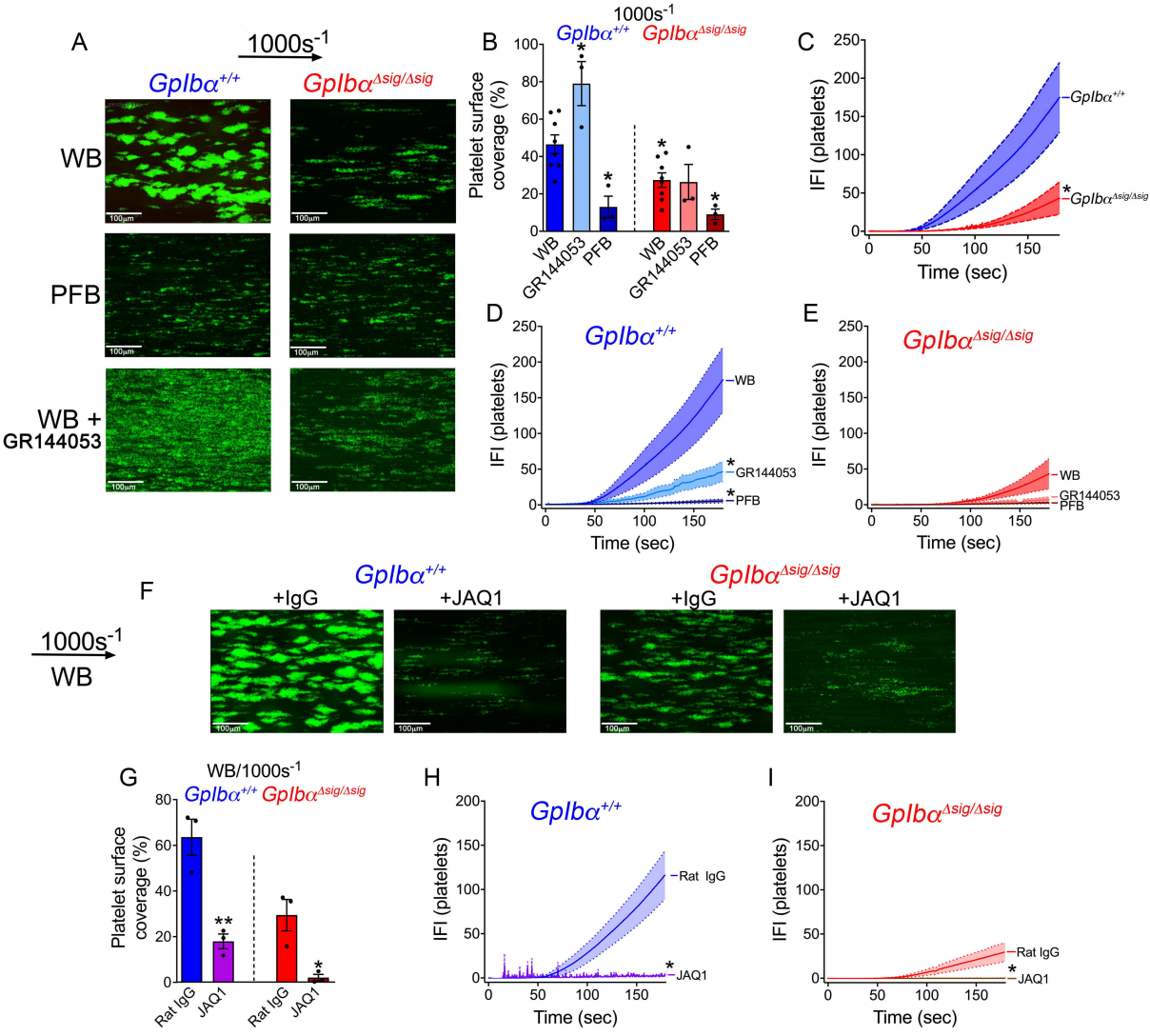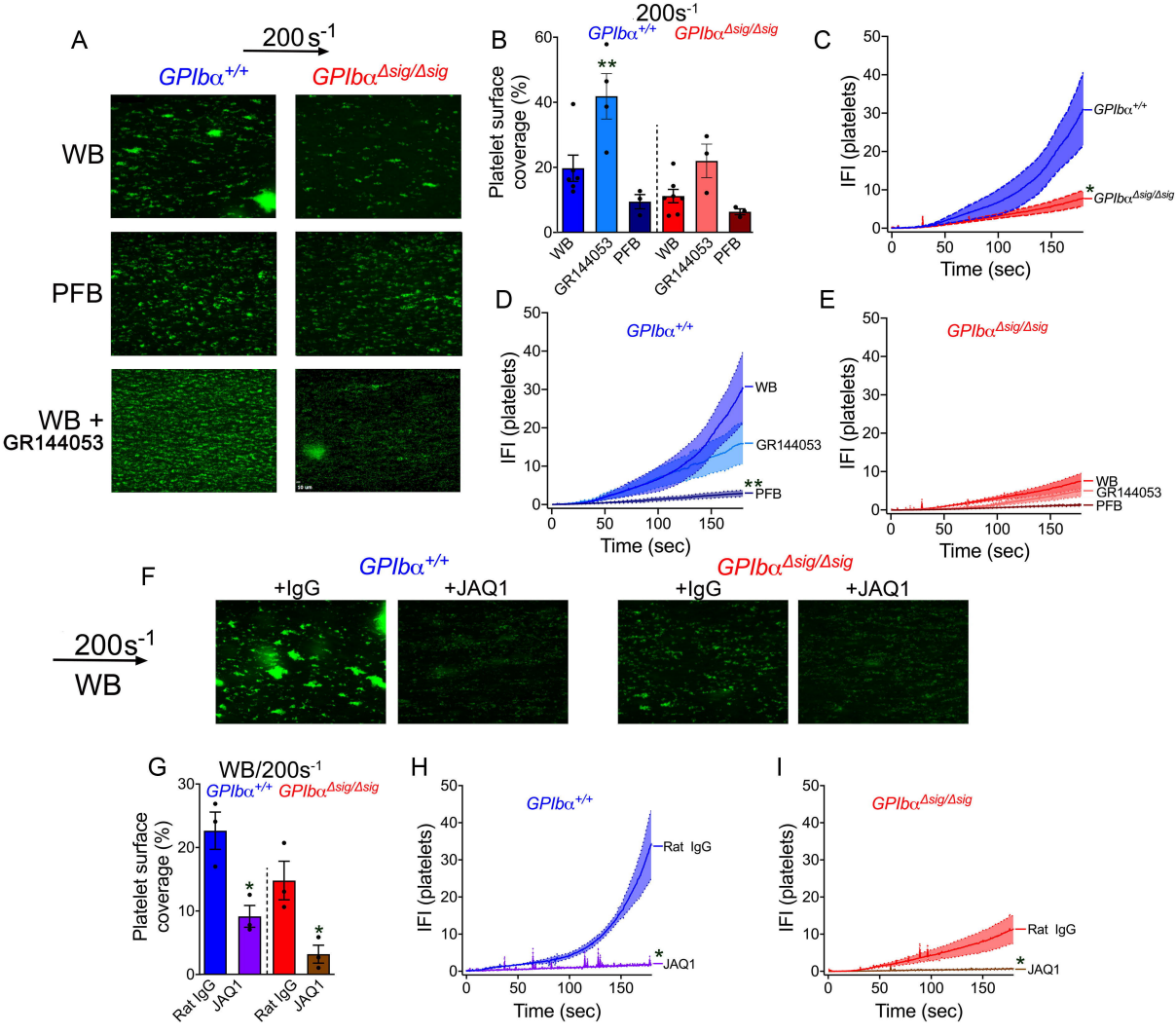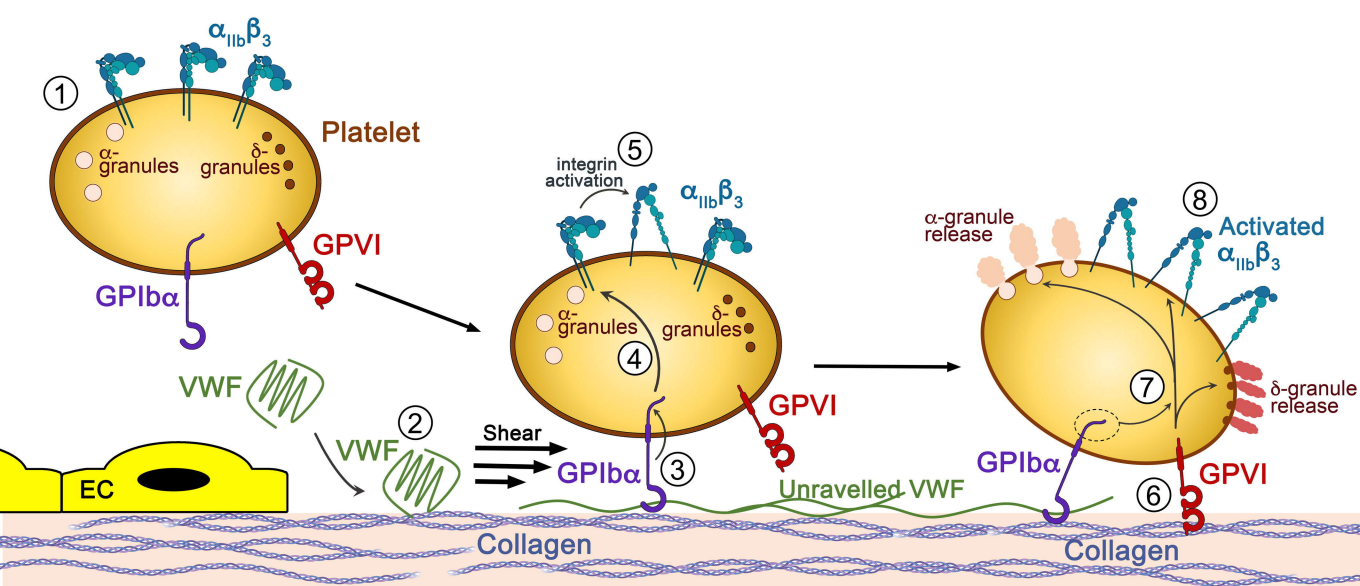$GPIb\alpha^{\Delta sig/\Delta sig}$

*

Time (sec)
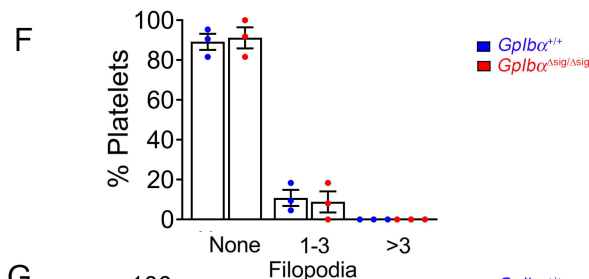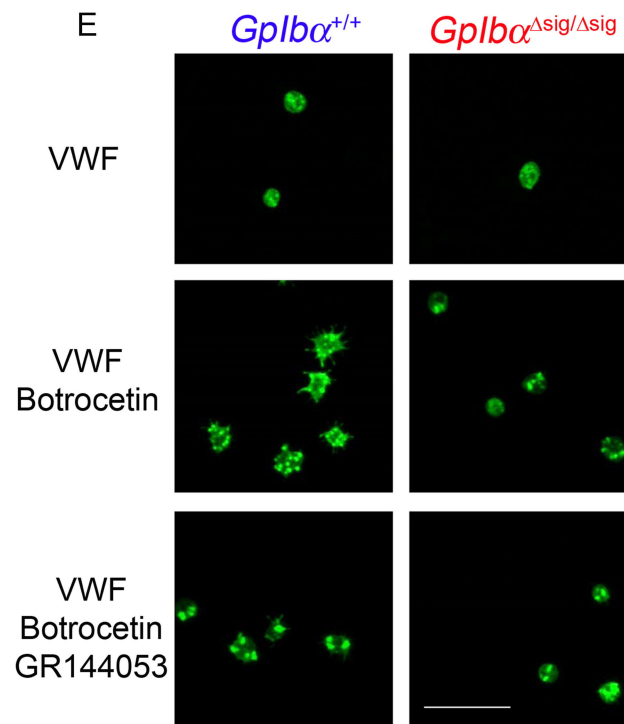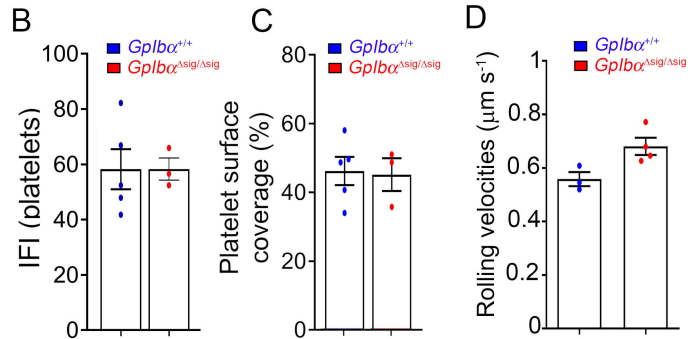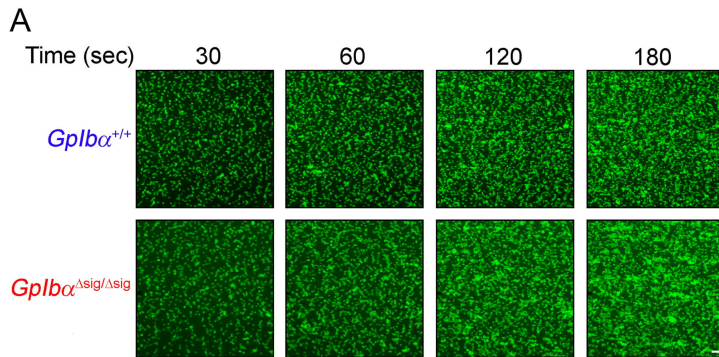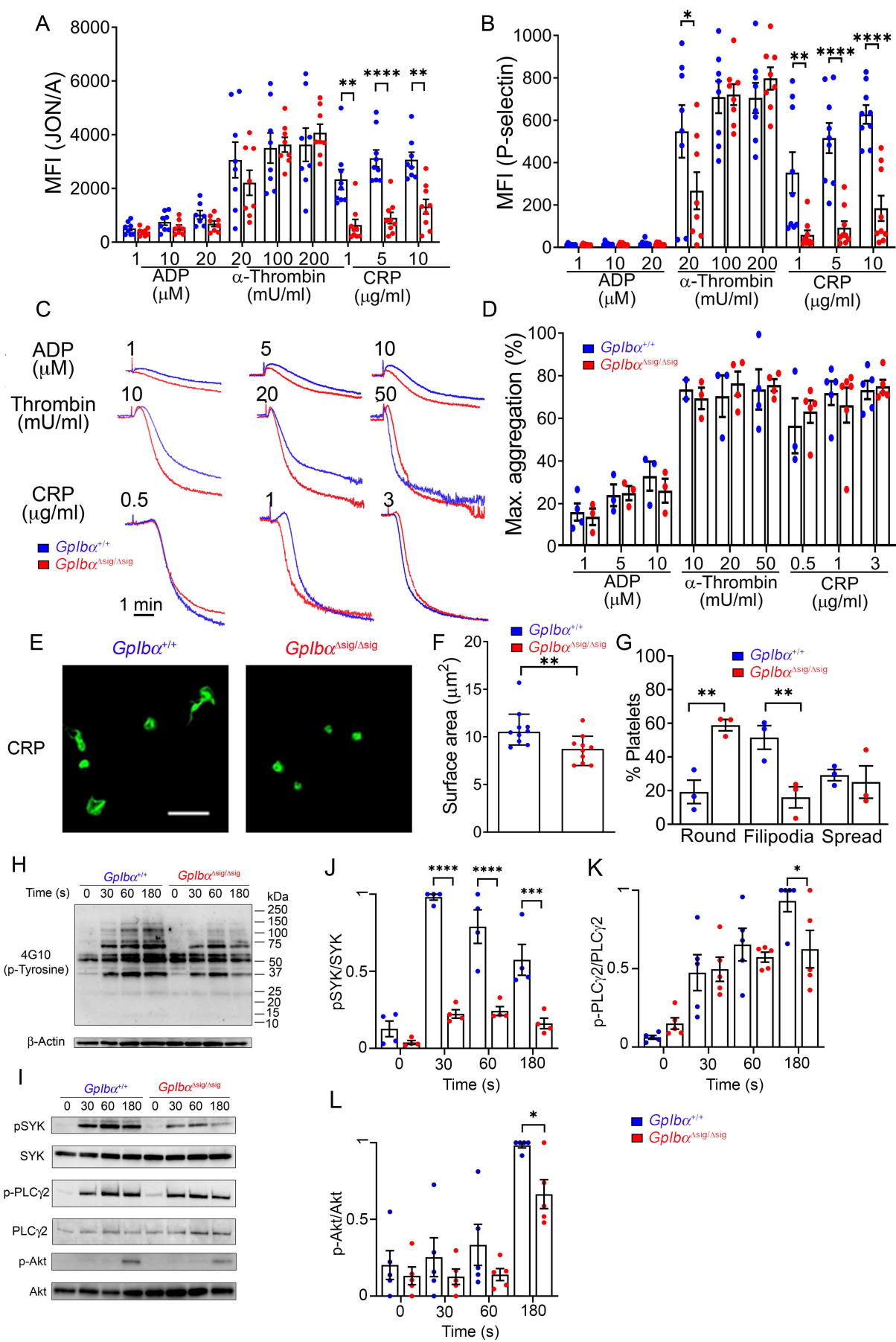
# SUPPLEMENTARY METHODS

**Determination of complete blood counts, platelet counts, surface protein expression and platelet activation.**

Mice were anaesthetized with ketamine/medetomidine and blood was collected retro-orbitally in 3.8% citrate. Blood was diluted with equal volume of saline and analyzed by the clinical pathology laboratory at Hammersmith Hospital to obtain full blood counts. Platelet counts were determined using precision count beads (Biolegend) and flow cytometry according to the manufacturer's instructions.

Platelets were washed as previously described with the following modifications.(1) Blood was diluted in an equal volume of modified Tyrode's buffer supplemented with prostaglandin E1 (PGE1) and apyrase (both from Sigma) and centrifuged at 150x$g$ for 10 mins at room temperature (RT). PRP was subsequently centrifuged at 1000x$g$ for 10 mins at RT and three additional centrifugation steps were performed to wash the platelets. Platelets were resuspended at $3 \times 10^5$ platelets/µl in modified Tyrode's buffer. In experiments using plasma-free blood, red blood cells and leukocytes were separately washed twice in PBS, by centrifugation at 650xg for 10 mins at RT and resuspended in Tyrode's buffer. Washed platelets were subsequently added to obtain plasma-free blood.

Flow cytometry was performed to analyze the surface expression of GPIb$\alpha$, GPIb$\beta$, $\alpha_{IIb}\beta_3$ and GPVI in platelets from *GpIb$\alpha^{\Delta sig/\Delta sig}$* and wild-type littermates using the following antibodies (Abs; Emfret): XiaB2, X488, Leo.H4, and JAQ1, respectively. Whole blood was diluted with modified Tyrode's buffer (1/20) and stained with Abs for 15 mins at RT before being analysed. Mouse platelets were washed as above and incubated with varying concentrations of agonists - ADP (2-20µM; Labmedics), thrombin (0.02-0.2U/ml; Enzyme Research Laboratories [ERL]), CRP (1-10µg/ml; Cambcol Laboratories), rhodocytin (3 and 300nM; kindly provided by Professor Eble and Dr Hughes) in the presence of 2mM CaCl$_2$ for 10 mins at RT. Thereafter, platelets were incubated with JON/A-PE and Wug.E9-FITC Abs for 15 mins at RT to analyze the surface expression of activated $\alpha_{IIb}\beta_3$ and P-selectin. Samples were analyzed using a BD LSRFortessa X-20 flow cytometer.

**Platelet aggregometry**

Platelet aggregation was assessed by light transmission using the Chronolog 700 aggregometer with continuous stirring at 1,200 rpm at 37°C. Washed platelets were resuspended to a final concentration of $3 \times 10^5$ platelets/µl in modified Tyrode's buffer and supplemented with 70µg/ml fibrinogen (ERL), 1mM CaCl$_2$ and different concentrations of ADP (1-10µM), $\alpha$-Thrombin (10-50mU/ml) or CRP (0.5-10µg/ml). Platelet aggregation was monitored over 6 mins.

**Platelet spreading**

Coverslips were coated with fibrinogen (200µg/ml), CRP (100µg/ml), murine VWF (10µg/ml) or BSA (0.5mg/ml) overnight at 4°C. Coverslips were then blocked with PBS-BSA (5mg/ml) for 1 hour at RT. Washed *GpIbα⁺ᐟ⁺* or *GpIbαᐞˢⁱᵍᐟᐞˢⁱᵍ* mouse platelets were added to the coverslips (150µl/coverslip, 25,000 platelets/µl) in the presence or absence of thrombin (1U/ml) or Botrocetin (2µg/ml) and allowed to adhere for 30 mins – 1 hour, at 37°C. When indicated, platelets were incubated with GR144053 (20µM) for 10 minutes to inhibit $\alpha_{IIb}\beta_3$ outside-in signaling prior to stimulation with Botrocetin. Coverslips were then washed with PBS, fixed with 10% formalin, and finally quenched with 50mM NH₄Cl-PBS. Platelets were then permeabilized in 0.1% Triton-PBS and stained with Flash Phalloidin™ Green 488 (2U/ml; Biolegend) for 1.5 hours, at RT. Finally, coverslips were mounted onto slides using ProLong™ Gold Antifade Mountant with DAPI (Thermofisher). Spread platelets were visualized using either a Vert.A1 inverted microscope (Zeiss; 40x and 63x air objectives) equipped with ExiBlue camera (Q Imaging) or a confocal microscope (SP5 Leica, 63x objective, z-stack, oil immersion). At least 3 fields of view were analyzed per condition. Surface area of spreading platelets was quantified using Slidebook software 5.0 (3i) and filopodia counted independently by two different researchers.

**Western blotting**

For analysis of GPVI and CLEC-2 tyrosine-mediated signaling pathways, washed platelets ($3 \times 10^5$ platelets/µl) were stimulated for the indicated time points with 3µg/ml CRP or 30 and 300nM rhodocytin, respectively. Samples were lysed with an equal volume of RIPA buffer (Sigma) supplemented with protease and phosphatase inhibitors (cOmplete, mini and PhosSTOP from Roche). The samples were run under reducing conditions with 4-12% Bolt™ Bis-Tris Plus or 4-20% Novex™ WedgeWell™ Tris-Glycine, 1.0 mm pre-cast gels and proteins were transferred to a nitrocellulose membrane. Membranes were blocked for 1 hour in 3% BSA-TBS and incubated overnight at 4°C with the following primary antibodies: anti-phosphotyrosine 4G10 (Millipore), anti-phosphorylated SYK (pY525/526; Abcam), anti-SYK (D1I5Q; Cell signaling Technology), anti-PLCγ2 (Cell signaling Technology), anti-phosphorylated PLCγ2 (pY1217; Cell signaling Technology), anti-β-actin (Cytoskeleton Inc.), anti-GAPDH (1D4; Novus Biological). The membranes were incubated with horseradish peroxidase-conjugated goat anti-mouse/rabbit secondary Abs (Dako) for 1h at RT and developed using Immobilon™ Western Chemiluminescent HRP Substrate (Millipore). Detection and quantification of chemiluminescence intensities were quantified by using Chemidoc™ imaging system. and Image Lab 5.2.1 software (BioRad).

**Flow assays**

Murine VWF was expressed in HEK293T cells, purified and quantified as previously described.(2) VenaFluoro8+ microchannels (Cellix) were coated directly with murine VWF (36.75µg/ml) or collagen (200µg/ml; Labmedics) overnight, at 4°C, in a humidified chamber. Channels were blocked for 1 hour, at RT with HEPES Tyrode's buffer (134mM NaCl, 0.3mM $Na_2HPO_4$, 2.9mM KCl, 12mM $NaHCO_3$, 20mM N-2-hydroxyethylpiperazine-N'-2-ethanesulfonic acid, 5mM Glucose, 1mM $MgCl_2$, pH 7.3) supplemented with 1% BSA.

On the day of the experiments, blood was collected retro-orbitally from *GpIbα*$^{Δsig/Δsig}$ mice and wild-type littermates in 100µg/ml Hirudin (Refludan, CSL Behring GmbH) and labelled with Dy-Light 488-conjugated rat anti-mouse GPIbβ (Emfret Analytics, 6µg/ml). When indicated, blood was incubated 5 min prior perfusion with GR144053 (10µM), anti-GPVI JAQ1 or control Rat IgG (Emfret; 20µg/ml). Thereafter, whole blood or plasma-free blood was perfused through the channels at 200-1000s$^{-1}$ using a Mirus pump (Cellix) for 3.5 mins and platelet adhesion/aggregate formation monitored in real-time by fluorescence microscopy (Vert.A1 inverted microscope, Zeiss), using an inverted CCD camera (ExiBlue from Q imaging) operated by the SlideBook$^{TM}$5.0 software. Quantification was performed using SlideBook 5.0 software (3i), to analyze platelet coverage, platelet velocity and thrombus build-up.

**Tail-bleeding assay**

Tail bleeding time was performed as described previously.(1, 3) Mice were anaesthetized with ketamine/medetomidine, placed on a heating pad (Harvard Apparatus) at 37°C and a 2 mm segment of the tail was sectioned with a sharp blade. The tail was immediately placed in warm PBS and the time taken for the stream of blood to stop for more than 60 seconds was defined as the bleeding time. To determine the extent of blood loss during the first 10 mins, hemoglobin content was determined by the colorimetric cyanmethemoglobin method using Drabkins reagent and bovine hemoglobin as a standard (Sigma).

**Laser-induced thrombosis model**

Thrombus formation was evaluated in the cremaster muscle microcirculation as previously described. (1, 3) Ketamine (75mg/kg) and medetomidine (1mg/kg) was initially given as an intraperitoneally injection. The anesthesia was maintained by giving additional ketamine (12.5mg/kg) every 40 mins. Briefly, Dy-Light 488-conjugated rat anti-mouse GPIbβ Ab (0.15µg/g;Emfret) and Alexa 647-conjugated fibrinogen (5% total fibrinogen; Invitrogen) were administered via a cannula inserted in the jugular vein. Vascular injury was induced by a pulse laser (Ablate!, 3i) focused through a 63X water-immersion objective (65-75% intensity, 5-15 pulses) leading to non-ablative/superficial injury.(4) No perforating injuries were performed under those conditions. Thrombus formation was

followed in real time for 3 mins after the injury. Median integrated fluorescence intensity over time from platelet or fibrin was determined and analyzed as detailed previously.(1, 3) The operator was blinded to the genotypes during both data acquisition and analysis.

**Statistical analysis**

Results are presented as mean ± SEM or median ± 95% confidence interval in accordance with their normality (Shapiro-Wilk) and analyzed using GraphPad Prism (8.01). Statistical analysis was performed using unpaired student t-test, the Mann-Whitney test or repeated measures ANOVA. Significance values are indicated in each figure legends.

SUPPLEMENTARY REFERENCES

1. Salles-Crawley I, Monkman JH, Ahnstrom J, Lane DA, Crawley JT. Vessel wall BAMBI contributes to hemostasis and thrombus stability [Research Support, N.I.H., Extramural

Research Support, Non-U.S. Gov't]. Blood. 2014 May 1;123(18):2873-81. eng. Epub 2014/03/15. doi:10.1182/blood-2013-10-534024. Cited in: Pubmed; PMID 24627527.

2. De Meyer SF, Budde U, Deckmyn H, Vanhoorelbeke K. In vivo von Willebrand factor size heterogeneity in spite of the clinical deficiency of ADAMTS-13. J Thromb Haemost. 2011 Dec;9(12):2506-8. Epub 2011/09/29. doi:10.1111/j.1538-7836.2011.04519.x. Cited in: Pubmed; PMID 21952041.

3. Crawley JTB, Zalli A, Monkman JH, Petri A, Lane DA, Ahnstrom J, Salles-Crawley I. Defective fibrin deposition and thrombus stability in Bambi(-/-) mice are mediated by elevated anticoagulant function. J Thromb Haemost. 2019 Nov;17(11):1935-1949. Epub 2019/07/28. doi:10.1111/jth.14593. Cited in: Pubmed; PMID 31351019.

4. Stalker TJ. Mouse laser injury models: variations on a theme. Platelets. 2020 May 18;31(4):423-431. Epub 2020/04/17. doi:10.1080/09537104.2020.1748589. Cited in: Pubmed; PMID 32297542.

## SUPPLEMENTARY TABLE

**Supplementary Table S1** Haematological parameters

|  | *GpIbα*$^{+/+}$ | *GpIbα*$^{\Delta sig/\Delta sig}$ |
|---|---|---|
| PLT ($10^3$/µl) | 1028 ± 187 | 818 ± 188**** |
| RBC ($10^6$/µl) | 9.0 ± 1.0 | 8.8 ± 0.7 |
| HCT (%) | 50.7 ± 5.2 | 49.7 ± 3.2 |
| WBC ($10^3$/µl) | 5.9 ± 1.8 | 6.7 ± 1.5 |

PLT, platelets; RBC, red blood cells; HCT, hematocrit, WBC, white blood cells; ****$P < 0.001$, unpaired, two-tailed t-test, mean ± SD (n=10 per genotype)
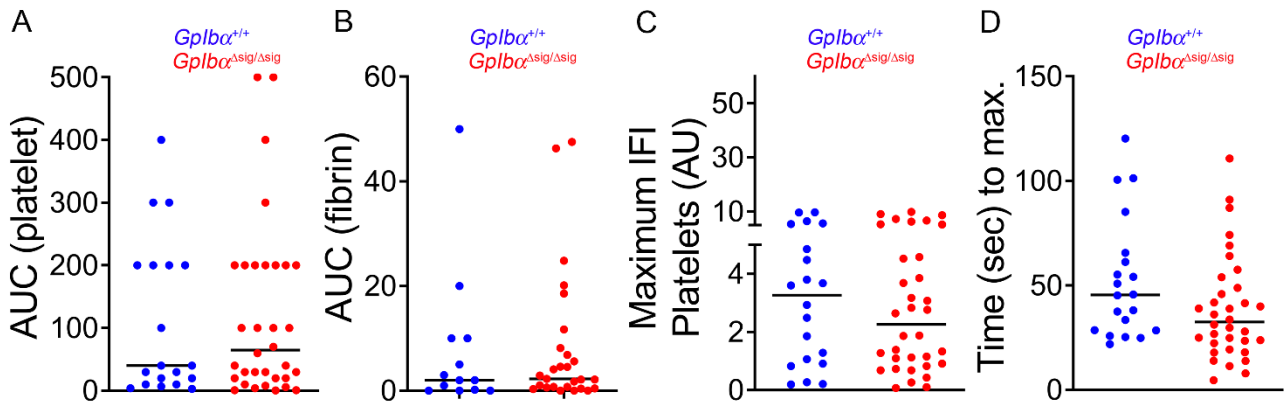
SUPPLEMENTARY FIGURES AND LEGENDS



**Figure S1: Thrombus formation and fibrin accumulation are similar in *GpIbα*<sup>Δsig/Δsig</sup> mice compared to *GpIbα*<sup>+/+</sup> mice.** Mice were subjected to the laser induced thrombosis model as detailed in Figure 2. Graphs showing the area under curve values from the platelet IFI (A) or fibrin(ogen) IFI (B) vs time from individual thrombus. (C) Distribution of the maximal thrombus size expressed in IFI platelet arbitrary units (AU) and (D) the time to maximal thrombus size. Each symbol represents one thrombus. Horizontal lines intersecting the data set represent the median. Data was analyzed using Mann Whitney test; ns: p>0.05. Also see Video 1 and Fig. 2.
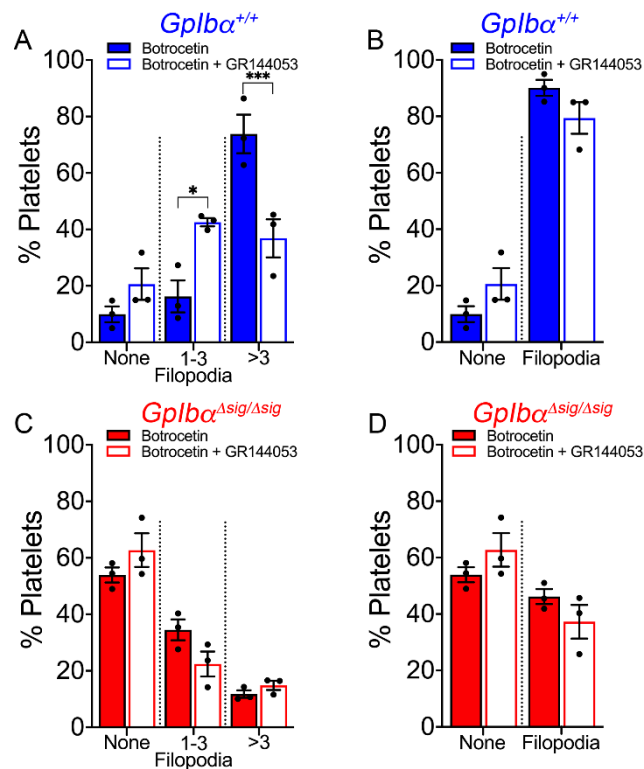
**Figure S2:** $GpIb\alpha^{\Delta sig/\Delta sig}$ **platelets exhibit disrupted GPIbα-mediated signaling.** $GpIb\alpha^{+/+}$ (A,B, blue bars) and $GpIb\alpha^{\Delta sig/\Delta sig}$ (C,D, red bars) platelets (n=3 for each genotype with individual data points representing the average of 3 fields of view) were spread on murine VWF and stained with Phalloidin-Alexa 488, in the presence of Botrocetin supplemented or not with GR144053. (A,C) Percentage of platelets from $GpIb\alpha^{+/+}$ and $GpIb\alpha^{\Delta sig/\Delta sig}$ mice with no filopodia, 1-3 filopodia or >3 filopodia formed on murine VWF upon stimulation with Botrocetin (511 $GpIb\alpha^{+/+}$ platelets and 547 $GpIb\alpha^{\Delta sig/\Delta sig}$ platelets analysed), or Botrocetin and GR144053 (359 $GpIb\alpha^{+/+}$ platelets and 480 $GpIb\alpha^{\Delta sig/\Delta sig}$ platelets analysed). (B,D) Percentage of platelets with or without filopodia formed on murine VWF upon stimulation with Botrocetin or Botrocetin and GR144053. All data is shown as mean ± SEM and was analyzed using two-way ANOVA followed by Sidak's multiple comparison test; *p<0.05, ***p<0.001. Also see Figure 2G-J.
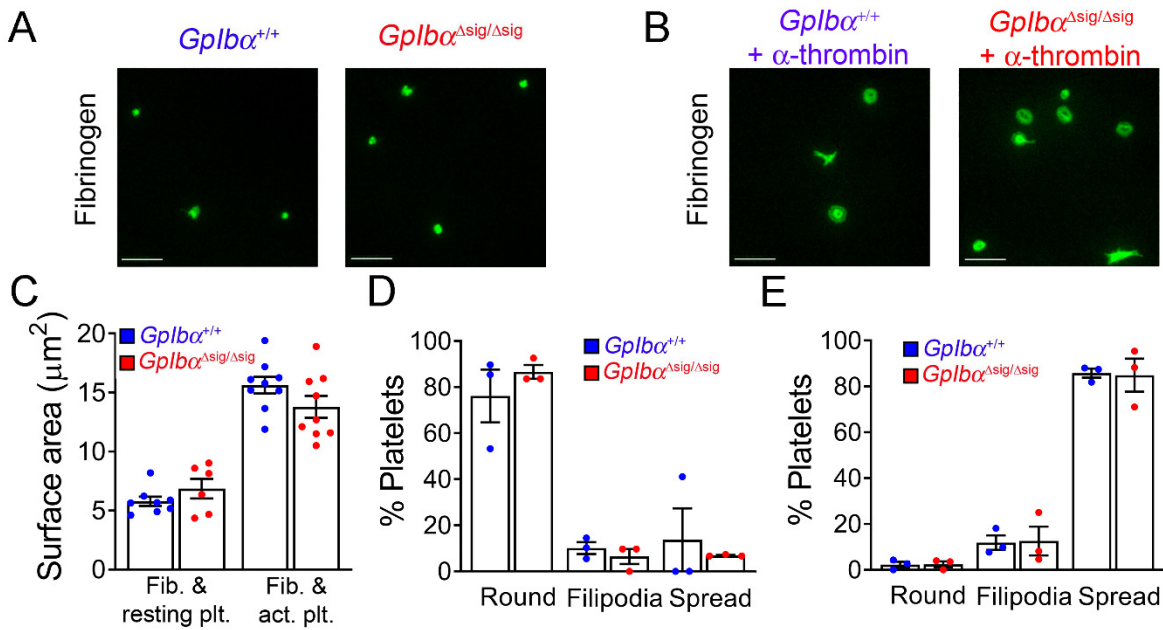
**Figure S3: *GpIbα^{Δsig/Δsig}* platelets spread normally on fibrinogen under basal and stimulated conditions.** Representative micrographs (n=3 for each genotype; 3 fields of view analyzed per condition; scale bar 10 μm) of *GpIbα^{+/+}* and *GpIbα^{Δsig/Δsig}* platelets in the absence (A; 131 *GpIbα^{+/+}* platelets and 86 *GpIbα^{Δsig/Δsig}* platelets analysed) or presence of 0.2U/ml α-thrombin (B; 264 *GpIbα^{+/+}* platelets and 497 *GpIbα^{Δsig/Δsig}* platelets analysed) and spread on fibrinogen. Platelet spreading was visualized by Phalloidin-Alexa 488 staining. Bar graphs quantifying the surface area (C) and percentages of platelets that remained round, formed filopodia or spread on fibrinogen under basal conditions (D) or activated with α-thrombin (E). The data represent the mean ± SEM and was analyzed using two-way ANOVA followed by Sidak's multiple comparison test; p>0.05. Fib.:fibrinogen; plt.: platelets; act.: α-thrombin-activated. Also see Figure 4A-G.
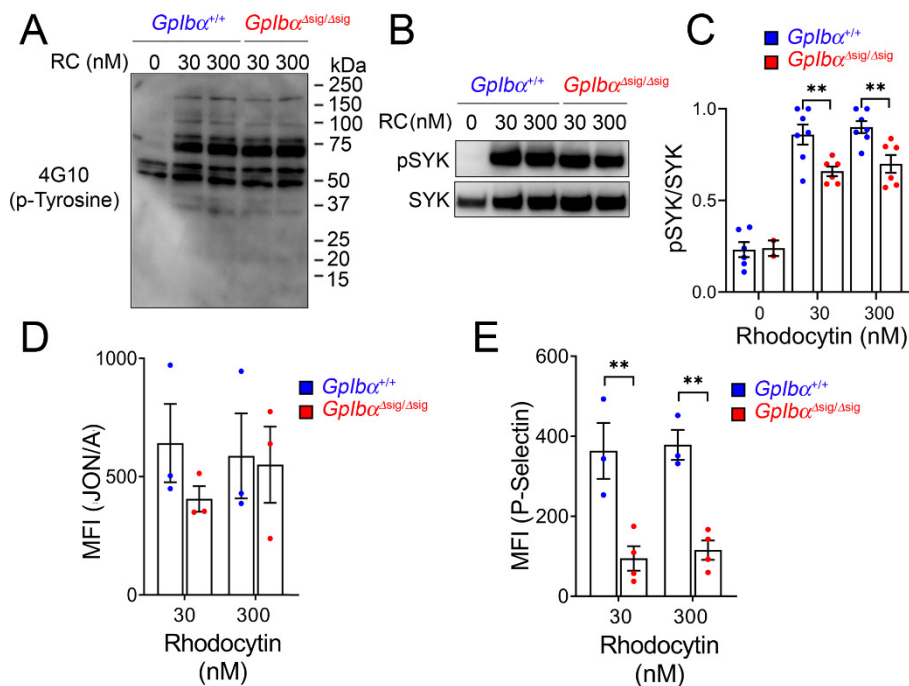
**Figure S4: Truncation of the GPIbα intracellular tail ~~does not greatly~~ influences CLEC-2 mediated signaling.** (A) Western blot analyzing tyrosine kinase phosphorylation in platelets from *GpIbα*^{+/+} and *GpIbα*[Δsig/Δsig] mice, following 5 min stimulation with rhodocytin (RC; 30 and 300nM), (representative of n=3). (B) Western blot and (C) bar graph analyzing the levels of phosphorylated and non-phosphorylated SYK in platelets from *GpIbα*^{+/+} and *GpIbα*[Δsig/Δsig] mice, after 5 mins stimulation with RC (representative of n=3). (D-E) Flow cytometric analysis of surface expression of activated $\alpha_{IIb}\beta_3$ (D) and P-selectin (E) in *GpIbα*^{+/+} and *GpIbα*[Δsig/Δsig] platelets (n≥3) after stimulation with rhodocytin (RC, 30-300nM). Data is shown as mean ± SEM and analyzed using two-way ANOVA followed by Sidak's multiple comparison test; \*\*p<0.001. Also see Figure 4H-L.

**Video 1 (separate file). Laser-induced thrombus formation in a *GpIbα$^{+/+}$* and *GpIbα$^{Δsig/Δsig}$* mouse:** Representative videos of fluorescently-labeled platelets (green) and fibrin(ogen) (red) accumulating at the site of laser-induced injury in a cremaster muscle arteriole of a *GpIbα$^{+/+}$* and *GpIbα$^{Δsig/Δsig}$* mouse. Thrombus formation was studied using a combination of brightfield and fluorescence microscopy. Results are presented in Figure 3. A timer is shown in the top left corner (hh:mm:ss:000) and a 10 μm scale bar in the bottom left corner.

**Video 2 (separate file). Platelet capture on murine VWF-coated microchannels.** Representative videos of hirudin-anticoagulated blood from a *GpIbα$^{+/+}$* and *GpIbα$^{Δsig/Δsig}$* mouse perfused over mouse VWF. Thrombus formation was visualized over 3 minutes of perfusion at 1000s$^{-1}$. Results are presented in Figure 2D-F. A timer is shown in the top left corner (hh:mm:ss:000) and a 10 μm scale bar in the bottom left corner.

**Video 3 (separate file). Formation of platelet aggregates on collagen-coated microchannels at 3000s$^{-1}$.** Representative video of hirudin-anticoagulated blood from a *GpIbα$^{+/+}$* and *GpIbα$^{Δsig/Δsig}$* mouse over fibrillar collagen type I. Thrombus formation was visualized over 3 minutes of perfusion at 3000s$^{-1}$. Results are presented in Figure 5. A timer is shown in the top left corner (hh:mm:ss:000) and a 10 μm scale bar in the bottom left corner.

**Video 4 (separate file). Formation of platelet aggregates on collagen-coated microchannels at 1000s$^{-1}$.** Representative video of hirudin-anticoagulated blood from a *GpIbα$^{+/+}$* and *GpIbα$^{Δsig/Δsig}$* mouse over fibrillar collagen type I. Thrombus formation was visualized over 3 minutes of perfusion at 1000s$^{-1}$. Results are presented in Figure 6. A timer is shown in the top left corner (hh:mm:ss:000) and a 10 μm scale bar in the bottom left corner.

**Video 5 (separate file). Formation of platelet aggregates on collagen-coated microchannels at 200s$^{-1}$.** Representative video of hirudin-anticoagulated blood from a *GpIbα$^{+/+}$* and *GpIbα$^{Δsig/Δsig}$* mouse over fibrillar collagen type I. Thrombus formation was visualized over 3 minutes of perfusion at 200s$^{-1}$. Results are presented in Figure 7. A timer is shown in the top left corner (hh:mm:ss:000) and a 10 μm scale bar in the bottom left corner.